Photophysical properties of halide perovskite $CsPb(Br_{1-x}I_x)_3$ thin films and nanowires

D.I. Markina,[1]* E.Yu. Tiguntseva,[1] A.P. Pushkarev,[1]* M.A. Samsonov,[2] M. Vengris,[3] B. Munkhbat,[4] T. Shegai,[4] G. Hix,[5] A.A. Zakhidov,[1,6] S.V. Makarov[1]

[1] *ITMO University, 197101 St.Petersburg, Russia*
[2] *University of Pardubice, 532 10 Pardubice, Czech Republic*
[3] *Vilnius University, Faculty of Physics, Laser Research Center, LT-10223 Vilnius, Lithuania*
[4] *Chalmers University of Technology, SE-412 96 Gothenburg, Sweden*
[5] *University of Wolverhampton, WV1 1LY Wolverhampton, United Kingdom*
[6] *The University of Texas at Dallas, Richardson, 75080 TX, USA*

Corresponding authors: D.I. Markina daria.markina@metalab.ifmo.ru, A.P. Pushkarev anatoly.pushkarev@metalab.ifmo.ru

Abstract: Thin films and nanowires based on lead halide perovskites are promising objects for the design of various optoelectronic devices as well as nano- and microlasers. One of the main advantages of such materials is their absorption and photoluminescence spectra tuning across the visible range via the change in their chemical composition, for instance, by substitution of one halide atom (Br) for another one (I) in the crystal lattice of $CsPb(Br_{1-x}I_x)_3$. However, this approach gives materials showing unstable photoluminescence behavior caused by light-induced perovskite phase separation under high-intensity excitation at room temperature. In this work, $CsPb(Br_{1-x}I_x)_3$ thin films and nanowires are obtained by chemical vapor anion exchange method from their $CsPbBr_3$ counterparts fabricated by improved wet chemical methods. Spontaneous and stimulated emission from the mixed-halide and pristine bromide samples are studied. Tribromide nanowires exhibit lasing with relatively low thresholds (10-100 μJ/cm^2) and high Q-factor of the laser mode up to 3500. The temperature dependence of the photoinitiated phase separation in $CsPbBr_{1.5}I_{1.5}$ samples is investigated, showing that light-induced phase instability of the mixed-halide nanowires can be suppressed at the somewhat higher temperature (250 K) than the value observed for the thin films having a similar chemical composition. The results obtained are important for the optimization of the functioning of optoelectronic devices based on considered perovskite materials.

Keywords: cesium lead halide perovskite, mixed-halide perovskite, thin film, nanowire, lasing, segregation

1. Introduction

Lead halide perovskites is a new class of perspective semiconductor materials demonstrating the photoluminescence (PL) quantum yield of about 90% [1] and fairly high charge carrier mobilities [2], that made it possible to fabricate solar cells showing a photoconversion efficiency of up to 25.2% [3] and light-emitting diodes with an electroluminescence efficiency of more than 20% [4] based on perovskite thin films. Moreover, perovskites have a relatively high value of dielectric permittivity in the visible range sufficient to support optical modes in their nano- and microstructures.[5] Such designs have been studied to create highly efficient and compact laser sources.[6–11] The main benefit of halide perovskites as functional components in optoelectronic devices is the possibility of tuning of their PL spectrum in the 410-800 nm range by varying the stoichiometric content of various

halogen ions in the $APbX_3$ structure (A = MA^+ - methylammonium, FA^+ - formamidine, Cs^+; X = Cl^-, Br^-, I^- or their binary mixtures). In the meanwhile, bulk mixed-halide perovskites are well known to be phase-unstable when illuminated with photons having energy greater than the band gap energy of the material. The nature of this instability lies in the segregation (migration) of photoactivated ions in the perovskite crystal lattice.[12] The segregation of halide ions results in the accumulation of the different ions in different perovskite domains. Thus, large band gap and low band gap domains are formed. The latter act as energetic funnels for the radiative recombination of photogenerated free charge carriers or excitons. The result of segregation and radiative recombination on the formed energetic funnels in mixed-halide perovskites is the dynamic tuning of their PL spectrum. Although this effect can be exploited for some specific purpose, stable photophysical properties of the perovskites still remain preferable for the development of the most common optoelectronic devices.

Herein we develop the techniques for deposition of high-quality $CsPbBr_3$ thin films and nanowires (NWs) as well as apply a chemical vapor anion exchange procedure to the samples to create the mixed-halide $CsPbBr_{1.5}I_{1.5}$ nanostructures. The tribromide films and NWs are illuminated with continuous UV light exhibit spontaneous emission at ca. 525 nm for studying their PL properties. Under femtosecond (fs) laser excitation (λ_{ex} = 351 nm, P = 10-100 μJ/cm^2) the NWs generate stimulated emission with a high Q-factor at lasing modes. Exposure of the films and NWs to HI vapor (5 μg/cm^3) at 150 ^{o}C for 10 and 30 s, respectively, results in their structural transformation to $CsPbBr_{1.5}I_{1.5}$ structures. The latter reveal light-induced phase instability which can be suppressed at the temperature lower than 250 K. The NWs demonstrate somewhat higher temperature at which there is no photoinitiated phase separation. This makes them more promising candidates in comparison with mixed-halide thin films for the design of perovskite-based photonic structures and devices with stable optical characteristics.

2. Results and discussion

2.1 Perovskite thin films deposition

Since lead halide perovskites of the $CsPbX_3$ type (X = Cl, Br, I) are ionic compounds capable of rapid formation of both mono- and polycrystalline micron and submicron objects under conditions of limited solubility of the corresponding CsX and PbX_2 precursors even in highly polar organic solvents such as DMSO (dimethyl sulfoxide) and DMF (N, N-dimethylformamide), deposition of their films with smooth surface morphology is challenging. One of the alternative approaches to obtain similar films of hybrid organic-inorganic perovskites ($MAPbX_3$, $FAPbX_3$; MA — methylammonium, FA — formamidinium) is the precipitation of small perovskite grains by dripping of perovskite anti-solvent onto the film surface during the spin-coating process.[13] Such a solvent (for example, diethyl ether, toluene, chlorobenzene, etc.) must be highly volatile and miscible with DMSO or DMF, providing them with the rapid evaporation from the volume of the perovskite precursors film or the perovskite itself. Rapid precipitation preferentially suppresses the growth of polycrystalline perovskite, substantially decreases the roughness of thin films, and minimizes the possibility of pinholes formation. It should be noted that the surface morphology of thin perovskite layers is crucial for the engineering of efficient optoelectronic devices[14] and its optimization in case of the different chemical composition may require different approaches. At the same time, the anti-solvent precipitation has an essential drawback consisting in the imperfect reproducibility of this procedure: the film morphology strongly depends on the dripping rate, the volume of

the anti-solvent, and its temperature. For this reason, we investigated another approach of the deposition of smooth thin $CsPbBr_3$ films.

$CsPbBr_3$ thin films on glass and Si substrates were fabricated by spin-casting at 2500 rpm for 300 s in a N_2-filled glove box (see *Materials and methods*). The images obtained by scanning electron microscopy confirm the formation of submicron grains with an average diameter size of 150 nm (Fig. S1) tightly adjacent to each other (Fig. 1a). The thickness and average roughness of tribromide films on a scale of 100 μm were determined by stylus profilometry and were found to be 80–82 nm and 3–4 nm, respectively (Fig. 1b). The X-ray diffraction pattern measured in the grazing incidence geometry exhibits peaks related to the orthorhombic phase of cesium lead tribromide.[15] The absence of peaks belonging to $PbBr_2$ in the spectrum indicates a complete conversion of lead(II) bromide to perovskite. In the meanwhile, the absence of doublet splitting of the lines at 2□ values of 15, 21, and 30 ° (Fig. 1c), which is well observed in the case of micron-size crystals, confirms that the films obtained consist of submicron crystallites. The elemental chemical composition of the samples was verified by quantitative X-ray photoelectron spectroscopy. The survey spectrum shown in Figure 1d reveals the characteristic radiation of the 3d and 3p subshells of the Br^- ion, 4f and 4d subshells of the Pb^{2+} cation and the 3d subshell of the Cs^+ ion. From the high-resolution spectra, Cs:Pb:Br ratio was derived to be close to 1.1:1:3.1, which coincides with 10% excess of cesium bromide taken in the reaction for the complete conversion of the $PbBr_2$ precursor to the $CsPbBr_3$ perovskite.

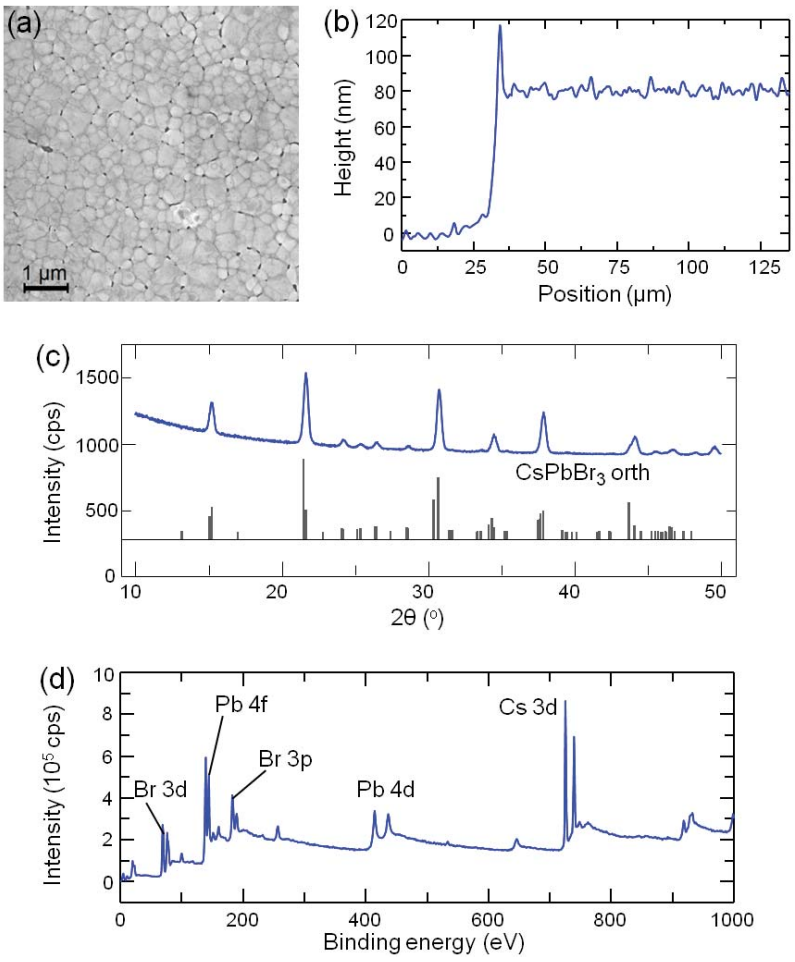

Figure 1. (a) Scanning electron microscopy image of the surface of $CsPbBr_3$ thin film deposited on a Si substrate. (b) The film profile measured with profilometry. (c) Diffraction pattern of the sample and the reference diffraction pattern for the orthorhombic $CsPbBr_3$.[15] (d) XPS survey spectrum of the sample.

The characterized $CsPbBr_3$ films were subjected to the rehalogenation (chemical vapor anion exchange or CVAE) of the perovskite crystal lattice [16] in hydrogen iodine vapor (see *Methods*) that can be described by the following chemical reaction:

$$y\ CsPbBr_3\ (s) + z\ HI\ (g) \leftrightarrows y\ CsPbBr_{3-x}I_x\ (s) + (z-xy)\ HI\ (g) + xy\ HBr\ (g),$$

where HI is taken in a significant excess as compared to generated HBr. For this reason, in the reaction, despite its reversibility, $CsPbBr_{3-x}I_x$ perovskite is formed. According to the position of the photoluminescence peak (see *Subsection 2.3*), the samples have a composition close to $CsPbBr_{1.5}I_{1.5}$.[17] Also, it was found that films kept in HI vapor but did not annealed afterwards, shows weak luminescence when illuminated with UV light. Apparently, the reason is multiple structural defects of the crystal lattice produced during anion exchange between the original tribromide films and HI vapor. Gradual annealing of the chemically modified samples from 150 to 320 °C leads to the elimination of lattice defects and, hence, to a multifold increase in the photoluminescence signal.

In addition to the structural modification of the samples evidently manifested itself in the change of their photophysical properties, it was important to determine how the rehalogenation procedure affects the surface morphology of the perovskite films. The data of high-resolution scanning electron microscopy revealed that initially smooth $CsPbBr_3$ grains possess a layered structure indicating the recrystallization of perovskite during the anion exchange reaction (Fig. S2). It is reasonable to assume that these layers possess different chemical composition, however, recently, a reaction between $CsPbBr_3$ films and HCl vapor was shown to yield similar layered grains and XRD patterns of the resulting $CsPbBr_{3-x}Cl_x$ films showed a set of single diffraction peaks corresponding to crystallographic phase of a certain perovskite lattice.[18] In the meanwhile, excitonic PL is supposed to be very sensitive to Br/I ratio in the perovskite structure and should exhibit a peak splitting or noticable spectral broadening in case if the ratio is not the same for each layer. PL peak of the $CsPbBr_{1.5}I_{1.5}$ film examined in our study has FWHM = 28 nm that is close to spectral width for similar perovskites reported by Beal et al [17] (see Supporting Information).

2.2 Perovskite nanowires deposition

Numerous studies have previously shown that lead halide NWs with length from a few to several tens of microns and lateral dimensions from 250 to 1000 nm can generate coherent stimulated emission in the entire visible spectral range. Positive feedback in such lasing structures is achieved due to the excitation of the Fabry-Perot modes in the volume of a NW. [7-11] Inorganic $CsPbX_3$ nano- and microlasers gain the following advantages over their organic-inorganic counterparts: they possess moderate resistance to oxygen, atmospheric moisture and high temperatures. As far as we know, several methods of perovskite NWs synthesis exist. The first method is to form a disordered forest of NWs from lead halide thin

film immersed in a solution of the corresponding cesium halide in absolutized methanol for 12 hours.[9] Another wet chemistry approach involves one-week cultivation of nanolasers from a DMF droplet containing precursor compounds that interact with a vapor of isopropyl alcohol (IPA, $(CH_3)_2CHOH$) in a sealed volume at room temperature. [10] The last method is the chemical vapor deposition (CVD) of NWs[11] which occurs in a controlled constant stream of pure N_2 or Ar gases and requires precise temperature control of the precursors' source. This makes CVD crystal growth not easy to access and implement.

Recently developed rapid, simple, and scalable solution-based method of $CsPbBr_3$ NWs synthesis [6] allows for formation of NWs from perovskite ink droplets sprayed onto hydrophobic substrates at ambient conditions and treated with IPA • H_2O azeotrope vapor at 50 ^oC for 5-7 min. In this work tribromide NWs were synthesized by using an improved approach detailed described in the *Materials and methods* section. It is worth noting that the deposition of ink droplets on the substrate is a necessary condition since the formation of NWs occurs in the diffusion layer between the ink droplet (the source of $PbBr_2$ and CsBr molecules) and the outer layer of alcohol-water condensate. The choice of alcohol-water azeotrope is also crucial. For example, utilization of methanol-water or ethanol-water azeotrope allows obtaining only a few NWs, whereas, in the case of employment an isopropanol-water mixture, the number of NWs precipitated on the substrate increases by 4-5 orders.

Since isopropanol is a protic solvent its molecules are predisposed to proton transfer to nearby water molecules. As a result of proton transfer anionic isopropoxide $[(CH_3)_2CHO]^-$ ligands and hydronium cations $[H_3O]^+$ are formed. The ligands have the geometric dimensions required for the effective passivation of the crystal seeds surface by forming weak covalent bonds with lead atoms, while $[H_3O]^+$ ions are located in the near-surface region in such a way to supply the neutral charge of the forming nanoobjects. Figure 2 shows $CsPbBr_3$ orthorhombic crystal lattice and the most probable location of the $[(CH_3)_2CHO]^-$ and $[H_3O]^+$ ions over the (001) perovskite crystallographic plane. The surface passivation of the crystallites prevents them from agglomeration and subsequent formation of polycrystalline precipitate. Further growth of individual crystals becomes possible due to the dynamic release and absorption of the generated ions by the perovskite surface. During their release, $PbBr_2$ and CsBr molecules are attached to the crystal seed. According to the structure of the presented crystal lattice (Fig. 2a), there is no significant difference between three considered orthogonal directions of its growth: [100], [010] and [001]. In this regard, it can be assumed that the shape of the formed nano- or microcrystal depends on the spatial orientation of planes of its seed relative to the reaction volume (or volumes) containing precursor molecules. $CsPbBr_{1.5}I_{1.5}$ NWs were obtained from tribromide structures in a similar way as mixed-halide perovskite films were (see *Materials and methods*).

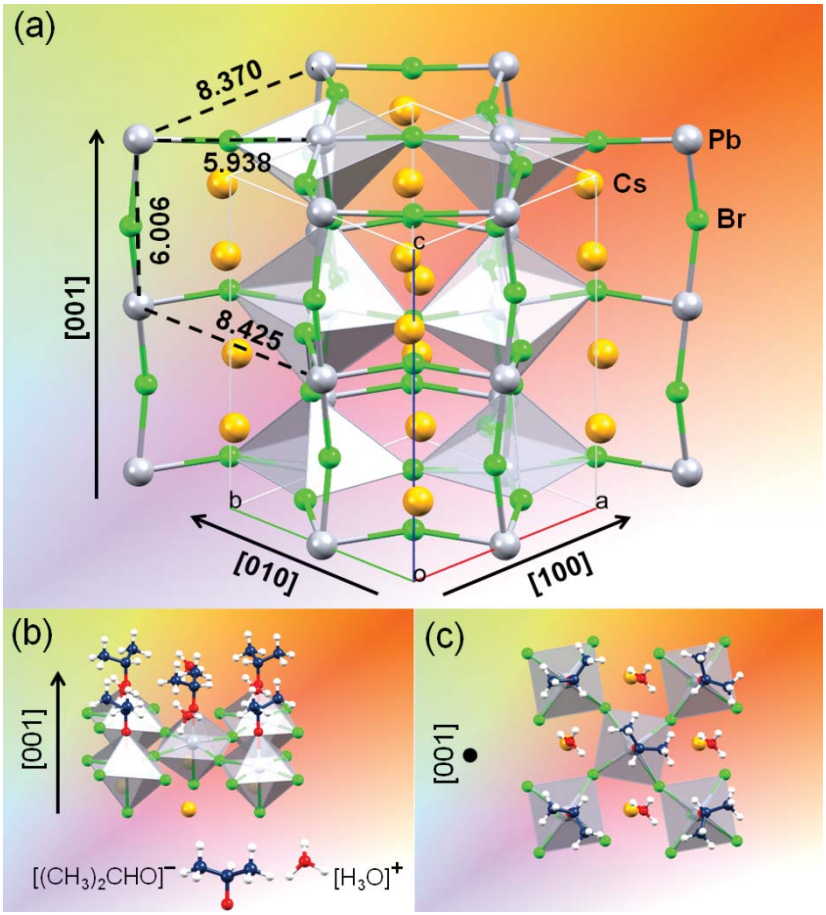

Figure 2. (a) Schematic representation of the $CsPbBr_3$ orthorhombic perovskite crystal lattice. The distances between Pb atoms are given in Å. The arrows indicate three crystallographic growth directions. (b-c) Location of isopropoxide ligands coordinated to surface lead atoms lying in the (001) plane and hydronium cations.

2.3 Photophysical properties of the samples

Under continuous wave UV (λ_{ex}=360 nm) irradiation $CsPbBr_3$ perovskite films and NWs show intense photoluminescence (PL) peaked at 525 nm. PL QY of the samples was estimated to be ≈34% (for films) and ≈83.4% (for array of NWs) at $4.3 \cdot 10^{15}$ cm^{-3} and 6×10^{16} cm^{-3} charge carrier densities, respectively (for details, see Materials and methods, and Supporting Information). When the same samples are excited by pulsed laser pump with a pulse duration of 150 fs, repetition frequency of 10 kHz and λ_{ex}=350 nm, NWs demonstrate narrow line-like stimulated emission in the range of 530–540 nm at relatively low thresholds of 10–100 μJ/cm^2 (Fig. 3). The spectral position of the laser peaks corresponds to Fabry-Perot modes of the cavity distributed over the gain in the region around the absorption edge. Integral PL intensity versus excitation power relationship shows typical ”S”-curve character (Fig. 3a). The number of laser modes, mode spacing (Δλ), and Q-factor (Q = λ/δλ, where δλ is the spectral bandwidth of a single laser line) of the laser mode depend on the length of the nanolaser.[5] For example, a spectrum of NW with sizes of 11.5x0.5x0.5 μm contains three lines. Each line consists of two laser modes with a quality factor of Q > 1700. The mode spacing was found to be approximately 1.85 nm (Fig. 3c). We also determined a crucial for

practical application parameter - critical fluence at which substantial photodamage is caused to nanolasers. Obviously, the cavities having large area cross-section are more robust to high power pumping. In particular, for a NW of nearly 10×0.5×0.5 μm size the fluence at which laser action is terminated was found to be about 200 μJ/cm^2.

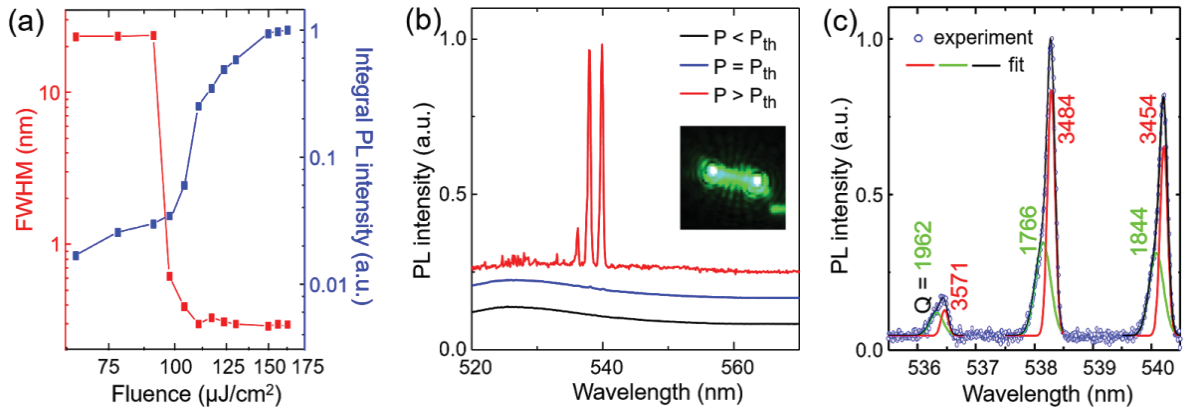

Figure 3. (a) Integral PL intensity and FWHM value versus excitation fluence relationship for 11.5 μm NW. (b) PL spectrum of the NW at different operation regimes (microphotograph of the acting nanolaser is presented in the inset image). (c) Gaussian fitting of the laser lines and Q-factors of the single modes.

Optical characteristics of mixed-halide perovskite samples were investigated in a similar way. It was found that under continuous weakly intense UV excitation films generate red light (λ_{em} = 630 nm) corresponding to the band gap energy $E_g \approx 2$ eV. Previously, Beal et al. reported a close value of E_g for $CsPbBr_{1.5}I_{1.5}$ perovskite.[17] In our experiments, PL QY of the iodine doped films at charge carrier density of ≈$4.3 \cdot 10^{15}$ cm^{-3} equals to 9% approximately. In contrast to films demonstrating identical PL signals from different points over the entire surface, the luminescence of various mixed-halide NWs differed significantly because of the different cross-section of the structures. Since the efficient anion exchange between the perovskite crystal lattice and HI vapor mainly occurs at the crystal surface, NWs possessing a large cross-section undergo nonequivalent chemical transformation in their volume. On the contrary, crystals with a small cross-section are capable of uniform rehalogenation of the bulk. Further gradual annealing of the samples in the 150-320 °C temperature range leads to the mixing of various halogens in the bulk due to ion diffusion and formation of a certain phase of the mixed-halide perovskite. In addition, the annealing eliminates the major part of structural defects. This allows $CsPbBr_{3-x}I_x$ NWs to generate relatively intense spontaneous emission but no stimulated emission since the remaining part of the defects introduces strong nonradiative dissipation channels for photogenerated charge carriers. It should also be mentioned that measuring the PL QY from an array of $CsPbBr_{3-x}I_x$ NWs of certain chemical composition is not possible for the samples exposed to HI vapor. Therefore, taking into account the difference in PL QY between the tribromide and mixed-halide films, $CsPbBr_{1.5}I_{1.5}$ NWs which are considered below is roughly assumed to possess 3.7 times lower value (≈22.5% at 6×10^{16} cm^{-3} charge carrier concentration) than that of $CsPbBr_3$ NWs.

When the mixed-halide samples were illuminated with intensive (P = 0.1 mW/μm^2) continuous wave (CW) light with photon energy above the band gap, they exhibited photoinduced phase instability resulting in the tuning of their PL spectrum over time. It was interesting to study the temperature dependence of the PL from mono- and mixed-halide

samples. For this purpose, a closed cycle cryostat and supercontinuum laser source with 488 and 532 nm bandpass filters for the excitation of $CsPbBr_3$ and $CsPbBr_{1.5}I_{1.5}$, respectively, were exploited. Cooling down the monohalide samples causes the following spectral changes: PL signal becomes narrower and more intensive while the position of the emission peak practically does not change (Fig. 4a, c). In the case of the $CsPbBr_{1.5}I_{1.5}$ film, it was found that the segregation effect manifesting itself in the appearance of two new emission bands in the spectrum at 620 and 680 nm is completely suppressed at 200 K (Fig. 4b). The short-wavelength light comes from perovskite domains enriched with Br^- ions, whereas long-wavelength emission is generated by domains with a high content of I^- ions.[19] In contrast to the mixed-halide film, NWs of similar chemical composition demonstrated no segregation effect at the temperature of 250 K (Fig. 4d). It is worth noting that when the excitation is removed the dark recovery of the light-induced phase separation proceeds in the same timescale as segregation evolves, which is 3-5 s for the mixed-halide films and NWs at 300 K, and about 7-8 min for the films cooled down to 250 K.

The observed difference between the temperatures at which mixed-halide phase of perovskite thin films and NWs becomes stable can be considered in terms of the crystal lattice defects diffusion. It is known that photoactivated halogen ions in halide perovskites migrate between lattice vacancies.[20] For this reason, the ion segregation rate is directly related to the diffusion rate of the vacancies determined in terms of diffusion coefficient $D = D_0\exp(-E_a/kT)$, where D_0 is a constant at $T \rightarrow \infty$, E_a is activation energy for vacancy diffusion, k is the Boltzmann constant. Furthermore, the concentration of vacancies also affects the segregation rate in an obvious way. From this point of view, initially monocrystalline perovskite NWs inherit a smaller number of defect states after the anion exchange procedure than polycrystalline thin films do. This explains enhanced resistance of the NWs against the ion segregation observed in the conducted experiments. Such a feature makes mixed-halide inorganic perovskite NWs attractive for the development of new photonic designs and optoelectronic devices emitting light over a wide spectral range.

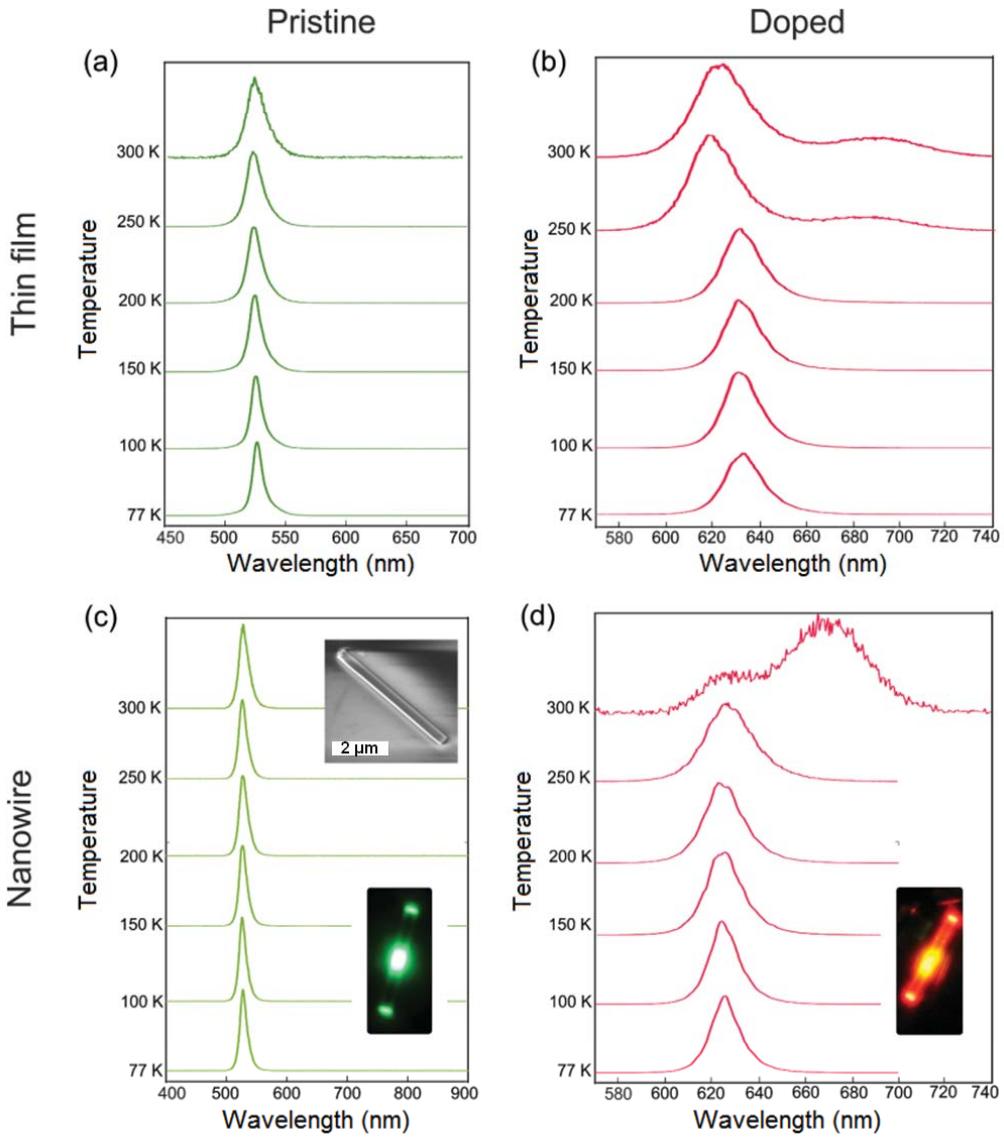

Figure 4. Dependence of the PL spectrum on temperature for $CsPbBr_3$ thin film (a) and NW (c) as well as for $CsPbBr_{1.5}I_{1.5}$ samples (b,d). Inset images: fluorescent microphotographs of the NW before (c) and after (d) the rehalogenation of its crystal structure; SEM image of the NW.

3. Conclusions

In summary, high-quality smooth thin films and monocrystalline nanowires of perovskite $CsPbBr_3$ have been fabricated by using improved wet chemical approaches. Additionally, the samples have been exposed to HI vapor to form related $CsPbBr_{1.5}I_{1.5}$ structures with narrower band gap. We have characterized all the obtained samples by means of scanning electron microscopy, stylus profilometry, X-ray photoelectron spectroscopy, X-ray powder diffraction, fluorescence and laser spectroscopy. The samples with mixed-halide composition have exhibited photoinduced phase instability upon continuous wave illumination, resulted in the dynamical modification of their optical characteristics, which can be suppressed under low temperature conditions. Since the phase instability is associated with the migration of photoactivated halogen ions (segregation) between perovskite lattice vacancies, the suppression of segregation at low temperatures occurs due to a decrease in the diffusion rate

of defect states. At the same time, perovskite NWs contain a lower concentration of structural vacancies than fine-grained films of the same chemical composition. For this reason, in comparison with thin films the stabilization of the phase and optical characteristics of mixed-halide perovskite nano- and microwires occurs at higher temperatures (about 250 K), that makes them promising materials for the development of new photonic designs and optoelectronic devices emitting light in the visible wavelength range.

3. Materials and methods

Materials. Lead(II) bromide ($PbBr_2$, 99.999%, Alfa Aesar), cesium bromide (CsBr, 99.999%, Sigma-Aldrich), dimethyl sulfoxide (DMSO, anhydrous, 99.8%, Alfa Aesar), isopropyl alcohol (IPA, technical grade, 95%, Vecton), hydrogen iodine (HI, 50%, Sigma-Aldrich) were used as received.

Preparation of perovskite ink. $PbBr_2$ (0.110 g, 0.3 mmol) and CsBr (0.07 g, 0.33 mmol) were dissolved in DMSO (3 ml) by shaking for 10 min to get a clear solution. Then the solution was filtered by using a 0.45 μm syringe filter with PTFE membrane. The chemicals were stored and mixed inside an N_2-filled glove box with both O_2 and H_2O level not exceeding 1 ppm.

$CsPbBr_3$ and $CsPbBr_{1.5}I_{1.5}$ thin films fabrication. Glass and hydrophobic silicon substrates were purchased from commercial suppliers. To make the substrates superhydrophilic, they were immersed in a piranha solution (mixture of 6 ml of sulfuric acid (H_2SO_4) and 2 ml of hydrogen peroxide (H_2O_2)) at 110 °C for 20 min. Afterwards substrates were carefully removed from the solution, rinsed with deionized water, dried with an air gun and then treated with ozone for 5 min.

To obtain high-quality films 30 μl of the perovskite ink was poured on the substrates and spin-coated at 2500 rpm for 300 s. To remove the residual DMSO molecules from the film, promote the complete conversion of the precursors to the target material $CsPbBr_3$, and eliminate the crystal lattice defects the deposited films were annealed gradually from 50 °C to 150 °C on a hot plate for 10 min.

In order to get thin films of mixed-halide composition, tribromide films were taken out of the glove box, then put in a Petri dish bottom and preheated with a glass piece lying close to the sample at 150 °C for 3 min. Afterwards, small amount of HI was dripped onto the glass piece and the sample with the glass were covered with the hot bottom of the weighing bottle. Thus the $CsPbBr_3$ film was exposed to hydrogen iodide vapor (5 μg/cm^3) at the temperature of 150 ˚C for 10 s. Finally, samples were gradually annealed in the 120–200 ˚C temperature range for 2 min to eliminate structural defects.

$CsPbBr_3$ and $CsPbBr_{1.5}I_{1.5}$ nanowires fabrication. The dissolved perovskite solution (0.1 M) was taken out from the glove box. The glass substrate was fixed in a plastic Petri dish bottom (35x9 mm) placed in a bigger glass one (80x15 mm) and preheated on the hotplate up to 50 °C. 0.5 μl of the ink was dripped onto a glass substrate with the formation of a small droplet. Immediately after that 100 μm of IPA•H_2O azeotrope was poured in the glass bottom and all the system was sealed. When the ink droplet increased in size due to the condensation of IPA•H_2O azeotrope on its surface, the substrate was tilted in such a way that the perovskite

droplet spreaded over the substrate leaving a trace. The trace was dried in the presence of IPA•H_2O azeotropic vapor for 1-2 min to give isolated high-quality NWs . This approach reduces the perovskite ink consumption and synthesis duration as compared to previously developed spray-casting at ambient conditions.[6]

To obtain NWs of the $CsPbBr_{1.5}I_{1.5}$ composition, the chemical vapor anion exchange method was used. The glass substrates with precipitated NWs were treated with HI vapor (5 μg/cm^3) at 150 °C for 30 s using the same construction as for chemical modification of the perovskite films. Afterwards, the samples were heated on a hotplate with a gradual increase in temperature from 150 to 320 °C for 2 minutes.

Structural characterization. Morphology of thin films and NWs were studied using a scanning electron microscope (Crossbeam 1540 XB, Carl Zeiss). High-resolution SEM images were obtained on FE-SEM-FIB HELIOS Nanolab 650 (FEI). Roughness of thin films was measured on a stylus profiler (P-7, KLA-Tencor). XRD patterns were measured using an X-ray diffractometer (SmartLab, Rigaku) equipped with a 9 kW rotating Cu anode X-ray tube. The measurements were performed using the grazing incidence (GIXRD) method in the 2θ range of 10-50°. The angle between the X-ray primary beam and the specimen surface was adjusted to 0.5°. XPS spectra were measured at $2.4x10^{-9}$ mbar pressure on X-ray photoelectron spectrometer system (Thermo Scientific K-Alpha) equipped with an Al source of monochromatic K-alpha X-ray (*hv* = 1486.6 eV). An energy scale was adjusted in accordance with Au 4f = 84 eV, Ag 3d = 368.2 eV and Cu 2p = 932.6 eV lines of standard samples. To neutralize a surface charge, a calibrated (C 1s = 284.8 eV) compensating electron flood gun was used. To obtain high-resolution (0.1 eV resolution) spectra, the x-ray beam was focused to 200 μm spot at constant pass energy of 50 eV and the number of scans of 10 was chosen.

Optical characterization. Spontaneous emission spectra of perovskite thin films and single NWs were recorded by using optical fiber spectrometer (Ocean Optics QE Pro) coupled with a microscope (Axio Imager A2m, Carl Zeiss) operating in the fluorescent regime. PL QY of perovskite thin films was measured in an integrating sphere under 368 nm CW excitation corresponding to photoexcited carrier density of ≈ $4.3{\cdot}10^{15}$ cm^{-3}. PL QY of $CsPbBr_3$ was derived from PL decay (Fig. S3) measured using the Edinburgh Instruments time-correlated single photon counting fluorescence spectrometer F900. The picosecond pulsed diode laser EPL-375 emitting 50 ps pulses at 375 nm with a repetition rate of 20 MHz was used for the sample excitation. The time resolution of the setup was found to be about hundred of picoseconds by applying apparatus function deconvolution.

Lasing from single NWs was investigated on a home-built optical setup (Fig. S4). Amplified femtosecond Yb:KGW laser (Pharos, Light Conversion) was used as an excitation source. Its output of 220 fs pulses arriving at 25 kHz repetition rate was frequency tripled in a home-built third harmonic generator and the resulting 343 nm beam was used to excite the sample. The excitation beam was focused onto the sample surface at normal incidence by the UV fused silica lens L1 (f=100 mm) which ensured a near-Gaussian excitation spot with a FWHM of 50 μm. The excitation pulse energy could be attenuated between 120 nJ and 1.2 nJ using a variable neutral density filter. The power was measured before the focusing lens L1 by a power meter (Ophir Nova2) equipped with a thermal power sensor (Ophir 3A). Emission of a single NW was collected in transmission configuration using 50× microscope objective (Mitutoyo M-Plan APO NUV, NA = 0.42) and passed through a long-pass filter with a cut-on

wavelength of 450 nm to block the excitation light. The emission was then directed into a high resolution spectrograph (Andor Shamrock SR-500i) equipped with a sensitive CCD camera (Andor iXON-DU-885). A grating of 1650 grooves/mm and input slit setting of 10-20 μm ensured the spectral resolution of around 45 pm. Sample positioning in the excitation beam was aided by a widefield microscope operated in epi-illumination arrangement, in which white LED served as an excitation source and a small color CCD camera (Point Grey Chameleon) was used to monitor the image through a beam splitter BS. Flipper mirror FM1 allowed switching between sample positioning and spectrum recording modes. All measurements were performed at ambient conditions.

Acknowledgment

The authors thank Dr. Vidas Pakštas, Arnas Naujokaitis, Filipp Komissarenko and Soslan Khubezhov for the help in the samples characterization. S.V.M. and A.A.Z. thank the Russian Science Foundation (grant 17-73-20336) for the financial support of study of nanostructures. S.V.M. acknowledges funding from the Ministry of Science and Higher Education of the Russian Federation (project 14.Y26.31.0010). M.V. acknowledges funding from the European Regional Development Fund according to the supported activity 'Research Projects Implemented by World-class Researcher Groups' under Measure No. 01.2.2-LMT-K-718, grant No. 01.2.2-LMT-K-718-01-0014. G.H. acknowledges ITMO Fellowship Program.

References:

[1] L. Protesescu, S. Yakunin, M.I. Bodnarchuk, F. Krieg, R. Caputo, C.H. Hendon, R.X. Yang, A. Walsh, and M.V. Kovalenko, Nano Lett. **15**, 3692 (2015).
[2] L.M. Herz, ACS Energy Lett. **2**, 1539 (2017).
[3] NREL. Efficiency chart. https://www.nrel.gov/pv/cell-efficiency.html
[4] W. Xu, Q. Hu, S. Bai, C. Bao, Y. Miao, Z. Yuan, T. Borzda, A.J. Barker, E. Tyukalova, Z. Hu, M. Kawecki, H. Wang, Z. Yan, X. Liu, X. Shi, K. Uvdal, M. Fahlman, W. Zhang, M. Duchamp, J.-M. Liu, A. Petrozza, J. Wang, L.-M. Liu, W. Huang, and F. Gao, Nature Photonics, (2019), DOI: 10.1038/s41566-019-0390-x.
[5] S. Makarov, A. Furasova, E. Tiguntseva, A. Hemmetter, A. Berestennikov, A. Pushkarev, A. Zakhidov, and Y. Kivshar, Adv. Opt. Mater. **7**, 1800784 (2019).
[6] A.P. Pushkarev, V.I. Korolev, D.I. Markina, F.E. Komissarenko, A. Naujokaitis, A. Drabavičius, V. Pakštas, M. Franckevičius, S.A. Khubezhov, D.A. Sannikov, A.V. Zasedatelev, P.G. Lagoudakis, A.A. Zakhidov, and S.V. Makarov, ACS Appl. Mater. Interfaces **11**, 1040 (2019).
[7] H. Zhu, Y. Fu, F. Meng, X. Wu, Z. Gong, Q. Ding, M.V. Gustafsson, M.T. Trinh, S. Jin, and X.-Y. Zhu, Nature Mater. **14**, 636 (2015).
[8] Y. Fu, H. Zhu, A.W. Schrader, D. Liang, Q. Ding, P. Joshi, L. Hwang, X.-Y. Zhu, and S. Jin, Nano Lett. **16**, 1000 (2016).
[9] S.W. Eaton, M. Lai, N.A. Gibson, A.B. Wong, L. Dou, J. Ma, L.-W. Wang, S.R. Leone, and P. Yang, PNAS **113**, 1993 (2016).
[10] L. Jiang, R. Liu, R. Su, Y. Yu, H. Xu, Y. Wei, Z.-K. Zhou, and X. Wang, Nanoscale **10**, 13565 (2018).
[11] K. Park, J.W. Lee, J.D. Kim, N.S. Han, D.M. Jang, S. Jeong, J. Park, and J.K. Song, J. Phys. Chem. Lett. **7**, 3703 (2016).
[12] E.T. Hoke, D.J. Slotcavage, E.R. Dohner, A.R. Bowring, H.I. Karunadasa, and M.D. McGehee, Chem. Sci. **6**, 613 (2015).

[13] N.J. Jeon, J.H. Noh, Y.C. Kim, W.S. Yang, S. Ryu, and S.I. Seok, Nature Materials **13**, 897 (2014).
[14] J. Li, X. Shan, S.G.R. Bade, T. Geske, Q. Jiang, X. Yang, and Z. Yu, J. Phys. Chem. Lett. **7**, 4059 (2016).tiguntseva
[15] M. Rodová, J. Brožek, K. Knížek, and K. Nitsch, J. Therm. Anal. Calorim. **71**, 667 (2003).
[16] E.Y. Tiguntseva, D.G. Baranov, A.P. Pushkarev, B. Munkhbat, F. Komissarenko, M. Franckevičius, A.A. Zakhidov, T. Shegai , Y.S. Kivshar, and S.V. Makarov, Nano Lett. **18**, 5522 (2018).
[17] R.E. Beal, D.J. Slotcavage, T. Leijtens, A.R. Bowring, R.A. Belisle, W.H. Nguyen, G.F. Burkhard, E.T. Hoke, and M.D. McGehee, J. Phys. Chem. Lett. **7**, 746 (2016).
[18] T.G. Liashenko, E.D. Cherotchenko, A.P. Pushkarev, V. Pakstas, A. Naujokaitis, S.A. Khubezhov, R.G. Polozkov, K.B. Agapev, A.A. Zakhidov, I.A. Shelykh, S.V. Makarov, Phys. Chem. Chem. Phys., 21, 18930 (2019)
[19] S.J. Yoon, S. Draguta, J.S. Manser, O. Sharia, W.F. Schneider, M. Kuno, and P.V. Kamat, ACS Energy Lett. **1**, 290 (2016).
[20] A. Ruth, M.C. Brennan, S. Draguta, Y.V. Morozov, M. Zhukovskyi, B. Janko, P. Zapol, and M. Kuno, ACS Energy Lett. **3**, 2321 (2018).

Supporting information

Photophysical properties of halide perovskite $CsPb(Br_{1-x}I_x)_3$ thin films and nanowires

D.I. Markina,[1]* E.Yu. Tiguntseva,[1] A.P. Pushkarev,[1] M.A. Samsonov,[2] M. Vengris,[3] B. Munkhbat,[4] T. Shegai,[4] G. Hix,[5] A.A. Zakhidov,[1,6] S.V. Makarov[1]

[1] ITMO University, 197101 St.Petersburg, Russia
[2] University of Pardubice, 532 10 Pardubice, Czech Republic
[3] Vilnius University, LT-10223 Vilnius, Lithuania
[4] Chalmers University of Technology, SE-412 96 Gothenburg, Sweden

[5] *University of Wolverhampton, WV1 1LY Wolverhampton, United Kingdom*
[6] *The University of Texas at Dallas, Richardson, 75080 TX, USA*

Corresponding author: D.I. Markina daria.markina@metalab.ifmo.ru , A.P. Pushkarev anatoly.pushkarev@metalab.ifmo.ru

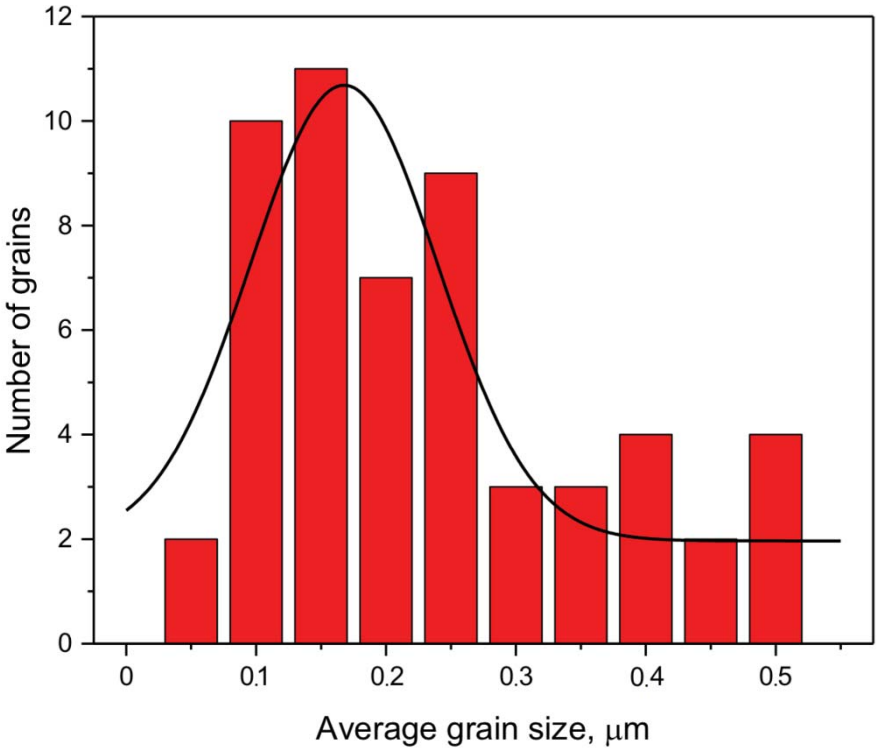

Figure S1. Average grain size distribution.

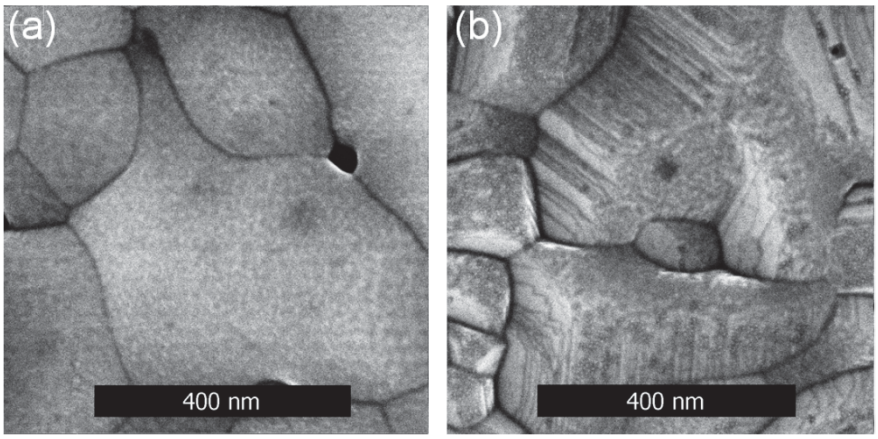

Figure S2. High-resolution SEM images of $CsPbBr_3$ (a) and $CsPbBr_{1.5}I_{1.5}$ (b) thin films.

S3. PL QY estimation for $CsPbBr_3$ NWs

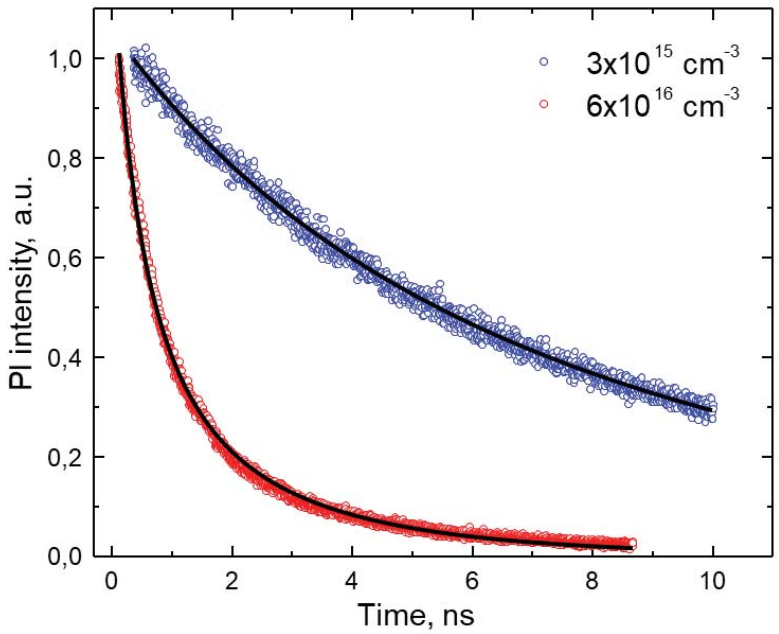

Figure S3. Photoluminescence decay of $CsPbBr_3$ NWs at different densities of the generated charge carriers.

PL QY of $CsPbBr_3$ NWs was estimated by using AB model discussed in detail in previous report.[7] The estimation is based on the fitting PL decay (Fig. S3) by fluence dependent bimolecular recombination function (1) from which, at given density of initially generated electron-hole pairs (n_0), a carrier trapping rate constant (A) and electron-hole radiative recombination rate constant (B) can be determined:

$$n(t) = \frac{n_0 \exp(-At)}{1 + n_0 \frac{B}{A}(1 - \exp(-At))}. \quad (1)$$

These constants are used to obtain PL QY (2) at n_0 lower than charge carriers concentration causing Auger recombination:

$$QY_{PL} = \frac{Bn_0}{A + Bn_0}. \quad (2)$$

n_0 is derived from the given excitation fluence, average thickness of the NWs which is about 0.5 μm, and attenuation coefficient $\alpha = \frac{4\pi}{\lambda} \mathrm{Im}(n(\omega))$ obtained from dispersion curves for $CsPbBr_3$.[16] It was found out, that carrier density ≈ 3×10^{15} cm^{-3} gives A = 9.2×10^{7} s^{-1}, B = 2.2×10^{-8} s^{-1} cm^3, and QY ≈ 41.7%, whereas n_0 ≈ 6×10^{16} cm^{-3} provides A = 2.94×10^{8} s^{-1}, B = 2.47×10^{-8} s^{-1} cm^3, and QY ≈ 83.4%.

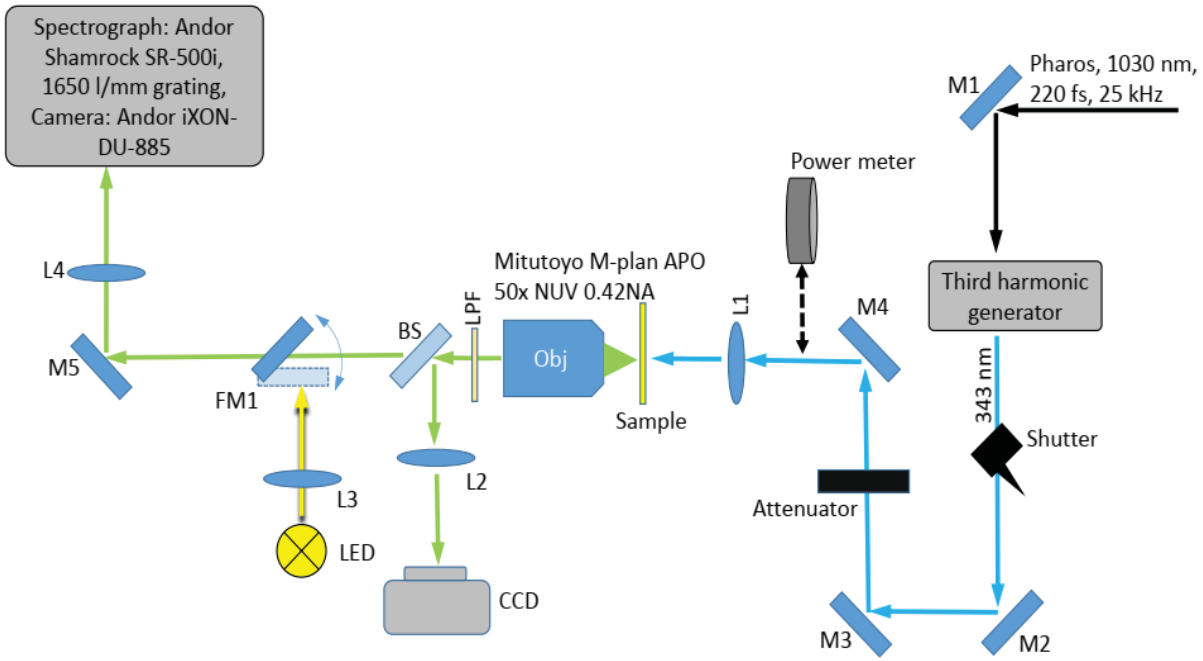

Figure S4. Schematic representation of the home-built optical setup employed for the detection of lasing from the perovskite nanowires. M1-M5: mirrors, Attenuator – variable neutral density filter, L1-L3 lenses, BS – beamsplitter, FM1 – flipper mirror.

1. No phase separation occurs at 200 K for $CsPbBr_{1.5}I_{1.5}$ films and 250 K for nanowires
2. CsPbBr3 nanowires show high Q-factor lasing (~3500) at low thresholds (10-100 $\mu J/cm^2$)
3. Nature of the phase instability is a migration of photoactivated ions in perovskite

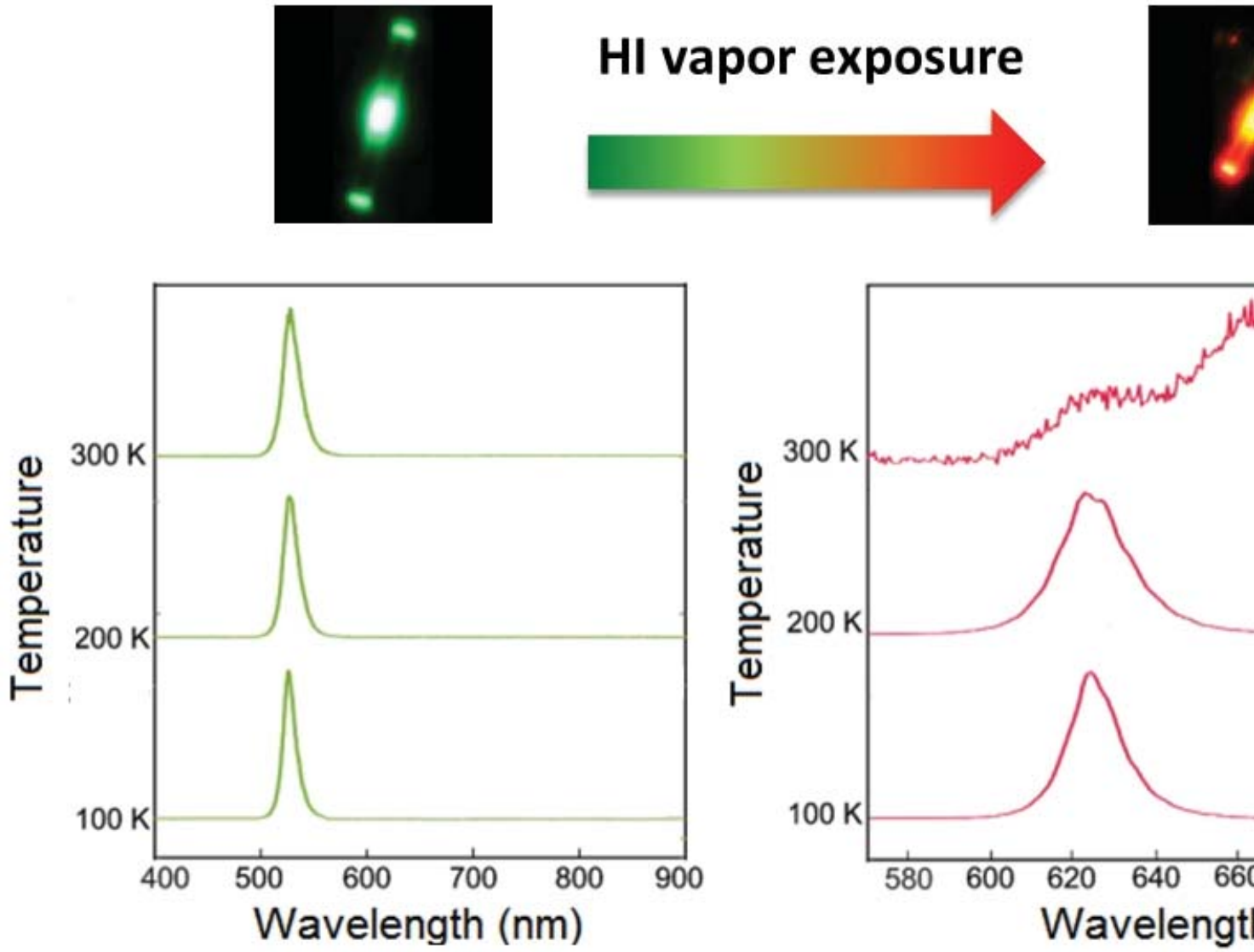
HI vapor exposure
Temperature
300 K
200 K
100 K
400
500
600
700
800
900
Wavelength (nm)
Temperature
300 K
200 K
100 K
580
600
620
640
660
Wavelengt

Photophysical properties of halide perovskite $CsPb(Br_{1-x}I_x)_3$ thin films and nanowires

D.I. Markina,[1]* E.Yu. Tiguntseva,[1] A.P. Pushkarev,[1]* M.A. Samsonov,[2] M. Vengris,[3] B. Munkhbat,[4] T. Shegai,[4] G. Hix,[5] A.A. Zakhidov,[1,6] S.V. Makarov[1]

[1] *ITMO University, 197101 St.Petersburg, Russia*
[2] *University of Pardubice, 532 10 Pardubice, Czech Republic*
[3] *Vilnius University, Faculty of Physics, Laser Research Center, LT-10223 Vilnius, Lithuania*
[4] *Chalmers University of Technology, SE-412 96 Gothenburg, Sweden*
[5] *University of Wolverhampton, WV1 1LY Wolverhampton, United Kingdom*
[6] *The University of Texas at Dallas, Richardson, 75080 TX, USA*

Corresponding authors: D.I. Markina daria.markina@metalab.ifmo.ru, A.P. Pushkarev anatoly.pushkarev@metalab.ifmo.ru

Abstract: Thin films and nanowires based on lead halide perovskites are promising objects for the design of various optoelectronic devices as well as nano- and microlasers. One of the main advantages of such materials is their absorption and photoluminescence spectra tuning across the visible range via the change in their chemical composition, for instance, by substitution of one halide atom (Br) for another one (I) in the crystal lattice of $CsPb(Br_{1-x}I_x)_3$. However, this approach gives materials showing unstable photoluminescence behavior caused by light-induced perovskite phase separation under high-intensity excitation at room temperature. In this work, $CsPb(Br_{1-x}I_x)_3$ thin films and nanowires are obtained by chemical vapor anion exchange method from their $CsPbBr_3$ counterparts fabricated by improved wet chemical methods. Spontaneous and stimulated emission from the mixed-halide and pristine bromide samples are studied. Tribromide nanowires exhibit lasing with relatively low thresholds (10-100 μJ/cm^2) and high Q-factor of the laser mode up to 3500. The temperature dependence of the photoinitiated phase separation in $CsPbBr_{1.5}I_{1.5}$ samples is investigated, showing that light-induced phase instability of the mixed-halide nanowires can be suppressed at the somewhat higher temperature (250 K) than the value observed for the thin films having a similar chemical composition. The results obtained are important for the optimization of the functioning of optoelectronic devices based on considered perovskite materials.

Keywords: cesium lead halide perovskite, mixed-halide perovskite, thin film, nanowire, lasing, segregation

1. Introduction

Lead halide perovskites is a new class of perspective semiconductor materials demonstrating the photoluminescence (PL) quantum yield of about 90% [1] and fairly high charge carrier mobilities [2], that made it possible to fabricate solar cells showing a photoconversion efficiency of up to 25.2% [3] and light-emitting diodes with an electroluminescence efficiency of more than 20% [4] based on perovskite thin films. Moreover, perovskites have a relatively high value of dielectric permittivity in the visible range sufficient to support optical modes in their nano- and microstructures.[5] Such designs have been studied to create highly efficient and compact laser sources.[6–11] The main benefit of halide perovskites as functional components in optoelectronic devices is the possibility of tuning of their PL spectrum in the 410-800 nm range by varying the stoichiometric content of various

halogen ions in the $APbX_3$ structure (A = MA^+ - methylammonium, FA^+ - formamidine, Cs^+; X = Cl^-, Br^-, I^- or their binary mixtures). In the meanwhile, bulk mixed-halide perovskites are well known to be phase-unstable when illuminated with photons having energy greater than the band gap energy of the material. The nature of this instability lies in the segregation (migration) of photoactivated ions in the perovskite crystal lattice.[12] The segregation of halide ions results in the accumulation of the different ions in different perovskite domains. Thus, large band gap and low band gap domains are formed. The latter act as energetic funnels for the radiative recombination of photogenerated free charge carriers or excitons. The result of segregation and radiative recombination on the formed energetic funnels in mixed-halide perovskites is the dynamic tuning of their PL spectrum. Although this effect can be exploited for some specific purpose, stable photophysical properties of the perovskites still remain preferable for the development of the most common optoelectronic devices.

Herein we develop the techniques for deposition of high-quality $CsPbBr_3$ thin films and nanowires (NWs) as well as apply a chemical vapor anion exchange procedure to the samples to create the mixed-halide $CsPbBr_{1.5}I_{1.5}$ nanostructures. The tribromide films and NWs are illuminated with continuous UV light exhibit spontaneous emission at ca. 525 nm for studying their PL properties. Under femtosecond (fs) laser excitation (λ_{ex} = 351 nm, P = 10-100 μJ/cm^2) the NWs generate stimulated emission with a high Q-factor at lasing modes. Exposure of the films and NWs to HI vapor (5 μg/cm^3) at 150 ^{o}C for 10 and 30 s, respectively, results in their structural transformation to $CsPbBr_{1.5}I_{1.5}$ structures. The latter reveal light-induced phase instability which can be suppressed at the temperature lower than 250 K. The NWs demonstrate somewhat higher temperature at which there is no photoinitiated phase separation. This makes them more promising candidates in comparison with mixed-halide thin films for the design of perovskite-based photonic structures and devices with stable optical characteristics.

2. Results and discussion

2.1 Perovskite thin films deposition

Since lead halide perovskites of the $CsPbX_3$ type (X = Cl, Br, I) are ionic compounds capable of rapid formation of both mono- and polycrystalline micron and submicron objects under conditions of limited solubility of the corresponding CsX and PbX_2 precursors even in highly polar organic solvents such as DMSO (dimethyl sulfoxide) and DMF (N, N-dimethylformamide), deposition of their films with smooth surface morphology is challenging. One of the alternative approaches to obtain similar films of hybrid organic-inorganic perovskites ($MAPbX_3$, $FAPbX_3$; MA — methylammonium, FA — formamidinium) is the precipitation of small perovskite grains by dripping of perovskite anti-solvent onto the film surface during the spin-coating process.[13] Such a solvent (for example, diethyl ether, toluene, chlorobenzene, etc.) must be highly volatile and miscible with DMSO or DMF, providing them with the rapid evaporation from the volume of the perovskite precursors film or the perovskite itself. Rapid precipitation preferentially suppresses the growth of polycrystalline perovskite, substantially decreases the roughness of thin films, and minimizes the possibility of pinholes formation. It should be noted that the surface morphology of thin perovskite layers is crucial for the engineering of efficient optoelectronic devices[14] and its optimization in case of the different chemical composition may require different approaches. At the same time, the anti-solvent precipitation has an essential drawback consisting in the imperfect reproducibility of this procedure: the film morphology strongly depends on the dripping rate, the volume of

the anti-solvent, and its temperature. For this reason, we investigated another approach of the deposition of smooth thin $CsPbBr_3$ films.

$CsPbBr_3$ thin films on glass and Si substrates were fabricated by spin-casting at 2500 rpm for 300 s in a N_2-filled glove box (see *Materials and methods*). The images obtained by scanning electron microscopy confirm the formation of submicron grains with an average diameter size of 150 nm (Fig. S1) tightly adjacent to each other (Fig. 1a). The thickness and average roughness of tribromide films on a scale of 100 μm were determined by stylus profilometry and were found to be 80–82 nm and 3–4 nm, respectively (Fig. 1b). The X-ray diffraction pattern measured in the grazing incidence geometry exhibits peaks related to the orthorhombic phase of cesium lead tribromide.[15] The absence of peaks belonging to $PbBr_2$ in the spectrum indicates a complete conversion of lead(II) bromide to perovskite. In the meanwhile, the absence of doublet splitting of the lines at 2□ values of 15, 21, and 30 ° (Fig. 1c), which is well observed in the case of micron-size crystals, confirms that the films obtained consist of submicron crystallites. The elemental chemical composition of the samples was verified by quantitative X-ray photoelectron spectroscopy. The survey spectrum shown in Figure 1d reveals the characteristic radiation of the 3d and 3p subshells of the Br^- ion, 4f and 4d subshells of the Pb^{2+} cation and the 3d subshell of the Cs^+ ion. From the high-resolution spectra, Cs:Pb:Br ratio was derived to be close to 1.1:1:3.1, which coincides with 10% excess of cesium bromide taken in the reaction for the complete conversion of the $PbBr_2$ precursor to the $CsPbBr_3$ perovskite.

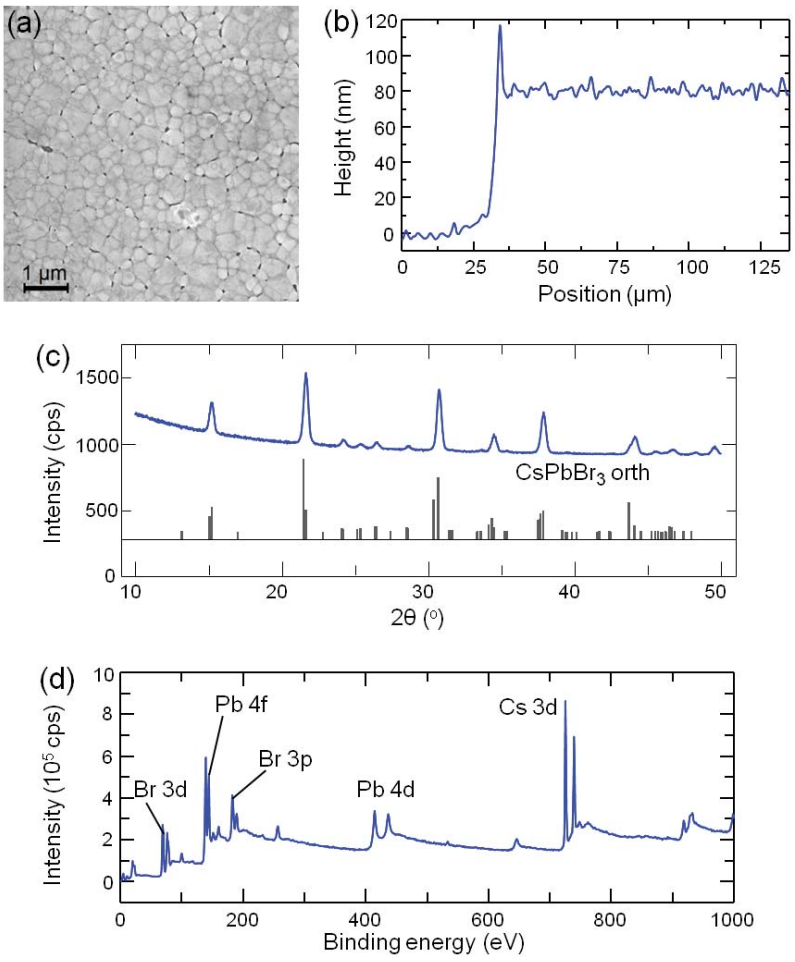

Figure 1. (a) Scanning electron microscopy image of the surface of $CsPbBr_3$ thin film deposited on a Si substrate. (b) The film profile measured with profilometry. (c) Diffraction pattern of the sample and the reference diffraction pattern for the orthorhombic $CsPbBr_3$.[15] (d) XPS survey spectrum of the sample.

The characterized $CsPbBr_3$ films were subjected to the rehalogenation (chemical vapor anion exchange or CVAE) of the perovskite crystal lattice [16] in hydrogen iodine vapor (see *Methods*) that can be described by the following chemical reaction:

$$y\ CsPbBr_3\ (s) + z\ HI\ (g) \leftrightarrows y\ CsPbBr_{3-x}I_x\ (s) + (z-xy)\ HI\ (g) + xy\ HBr\ (g),$$

where HI is taken in a significant excess as compared to generated HBr. For this reason, in the reaction, despite its reversibility, $CsPbBr_{3-x}I_x$ perovskite is formed. According to the position of the photoluminescence peak (see *Subsection 2.3*), the samples have a composition close to $CsPbBr_{1.5}I_{1.5}$.[17] Also, it was found that films kept in HI vapor but did not annealed afterwards, shows weak luminescence when illuminated with UV light. Apparently, the reason is multiple structural defects of the crystal lattice produced during anion exchange between the original tribromide films and HI vapor. Gradual annealing of the chemically modified samples from 150 to 320 °C leads to the elimination of lattice defects and, hence, to a multifold increase in the photoluminescence signal.

In addition to the structural modification of the samples evidently manifested itself in the change of their photophysical properties, it was important to determine how the rehalogenation procedure affects the surface morphology of the perovskite films. The data of high-resolution scanning electron microscopy revealed that initially smooth $CsPbBr_3$ grains possess a layered structure indicating the recrystallization of perovskite during the anion exchange reaction (Fig. S2). It is reasonable to assume that these layers possess different chemical composition, however, recently, a reaction between $CsPbBr_3$ films and HCl vapor was shown to yield similar layered grains and XRD patterns of the resulting $CsPbBr_{3-x}Cl_x$ films showed a set of single diffraction peaks corresponding to crystallographic phase of a certain perovskite lattice.[18] In the meanwhile, excitonic PL is supposed to be very sensitive to Br/I ratio in the perovskite structure and should exhibit a peak splitting or noticable spectral broadening in case if the ratio is not the same for each layer. PL peak of the $CsPbBr_{1.5}I_{1.5}$ film examined in our study has FWHM = 28 nm that is close to spectral width for similar perovskites reported by Beal et al [17] (see Supporting Information).

2.2 Perovskite nanowires deposition

Numerous studies have previously shown that lead halide NWs with length from a few to several tens of microns and lateral dimensions from 250 to 1000 nm can generate coherent stimulated emission in the entire visible spectral range. Positive feedback in such lasing structures is achieved due to the excitation of the Fabry-Perot modes in the volume of a NW. [7-11] Inorganic $CsPbX_3$ nano- and microlasers gain the following advantages over their organic-inorganic counterparts: they possess moderate resistance to oxygen, atmospheric moisture and high temperatures. As far as we know, several methods of perovskite NWs synthesis exist. The first method is to form a disordered forest of NWs from lead halide thin

film immersed in a solution of the corresponding cesium halide in absolutized methanol for 12 hours.[9] Another wet chemistry approach involves one-week cultivation of nanolasers from a DMF droplet containing precursor compounds that interact with a vapor of isopropyl alcohol (IPA, $(CH_3)_2CHOH$) in a sealed volume at room temperature. [10] The last method is the chemical vapor deposition (CVD) of NWs[11] which occurs in a controlled constant stream of pure N_2 or Ar gases and requires precise temperature control of the precursors' source. This makes CVD crystal growth not easy to access and implement.

Recently developed rapid, simple, and scalable solution-based method of $CsPbBr_3$ NWs synthesis [6] allows for formation of NWs from perovskite ink droplets sprayed onto hydrophobic substrates at ambient conditions and treated with IPA • H_2O azeotrope vapor at 50 ^oC for 5-7 min. In this work tribromide NWs were synthesized by using an improved approach detailed described in the *Materials and methods* section. It is worth noting that the deposition of ink droplets on the substrate is a necessary condition since the formation of NWs occurs in the diffusion layer between the ink droplet (the source of $PbBr_2$ and CsBr molecules) and the outer layer of alcohol-water condensate. The choice of alcohol-water azeotrope is also crucial. For example, utilization of methanol-water or ethanol-water azeotrope allows obtaining only a few NWs, whereas, in the case of employment an isopropanol-water mixture, the number of NWs precipitated on the substrate increases by 4-5 orders.

Since isopropanol is a protic solvent its molecules are predisposed to proton transfer to nearby water molecules. As a result of proton transfer anionic isopropoxide $[(CH_3)_2CHO]^-$ ligands and hydronium cations $[H_3O]^+$ are formed. The ligands have the geometric dimensions required for the effective passivation of the crystal seeds surface by forming weak covalent bonds with lead atoms, while $[H_3O]^+$ ions are located in the near-surface region in such a way to supply the neutral charge of the forming nanoobjects. Figure 2 shows $CsPbBr_3$ orthorhombic crystal lattice and the most probable location of the $[(CH_3)_2CHO]^-$ and $[H_3O]^+$ ions over the (001) perovskite crystallographic plane. The surface passivation of the crystallites prevents them from agglomeration and subsequent formation of polycrystalline precipitate. Further growth of individual crystals becomes possible due to the dynamic release and absorption of the generated ions by the perovskite surface. During their release, $PbBr_2$ and CsBr molecules are attached to the crystal seed. According to the structure of the presented crystal lattice (Fig. 2a), there is no significant difference between three considered orthogonal directions of its growth: [100], [010] and [001]. In this regard, it can be assumed that the shape of the formed nano- or microcrystal depends on the spatial orientation of planes of its seed relative to the reaction volume (or volumes) containing precursor molecules. $CsPbBr_{1.5}I_{1.5}$ NWs were obtained from tribromide structures in a similar way as mixed-halide perovskite films were (see *Materials and methods*).

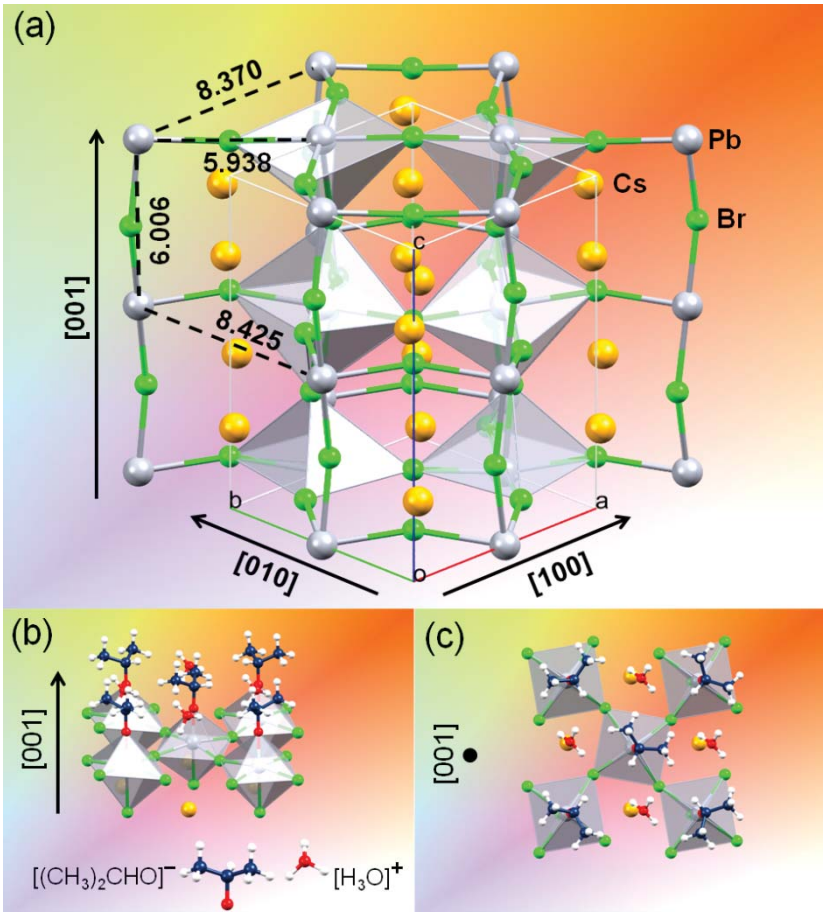

Figure 2. (a) Schematic representation of the $CsPbBr_3$ orthorhombic perovskite crystal lattice. The distances between Pb atoms are given in Å. The arrows indicate three crystallographic growth directions. (b-c) Location of isopropoxide ligands coordinated to surface lead atoms lying in the (001) plane and hydronium cations.

2.3 Photophysical properties of the samples

Under continuous wave UV (λ_{ex}=360 nm) irradiation $CsPbBr_3$ perovskite films and NWs show intense photoluminescence (PL) peaked at 525 nm. PL QY of the samples was estimated to be ≈34% (for films) and ≈83.4% (for array of NWs) at $4.3 \cdot 10^{15}$ cm^{-3} and 6×10^{16} cm^{-3} charge carrier densities, respectively (for details, see Materials and methods, and Supporting Information). When the same samples are excited by pulsed laser pump with a pulse duration of 150 fs, repetition frequency of 10 kHz and λ_{ex}=350 nm, NWs demonstrate narrow line-like stimulated emission in the range of 530–540 nm at relatively low thresholds of 10–100 μJ/cm^2 (Fig. 3). The spectral position of the laser peaks corresponds to Fabry-Perot modes of the cavity distributed over the gain in the region around the absorption edge. Integral PL intensity versus excitation power relationship shows typical ”S”-curve character (Fig. 3a). The number of laser modes, mode spacing (Δλ), and Q-factor (Q = λ/δλ, where δλ is the spectral bandwidth of a single laser line) of the laser mode depend on the length of the nanolaser.[5] For example, a spectrum of NW with sizes of 11.5x0.5x0.5 μm contains three lines. Each line consists of two laser modes with a quality factor of Q > 1700. The mode spacing was found to be approximately 1.85 nm (Fig. 3c). We also determined a crucial for

practical application parameter - critical fluence at which substantial photodamage is caused to nanolasers. Obviously, the cavities having large area cross-section are more robust to high power pumping. In particular, for a NW of nearly 10×0.5×0.5 μm size the fluence at which laser action is terminated was found to be about 200 μJ/cm^2.

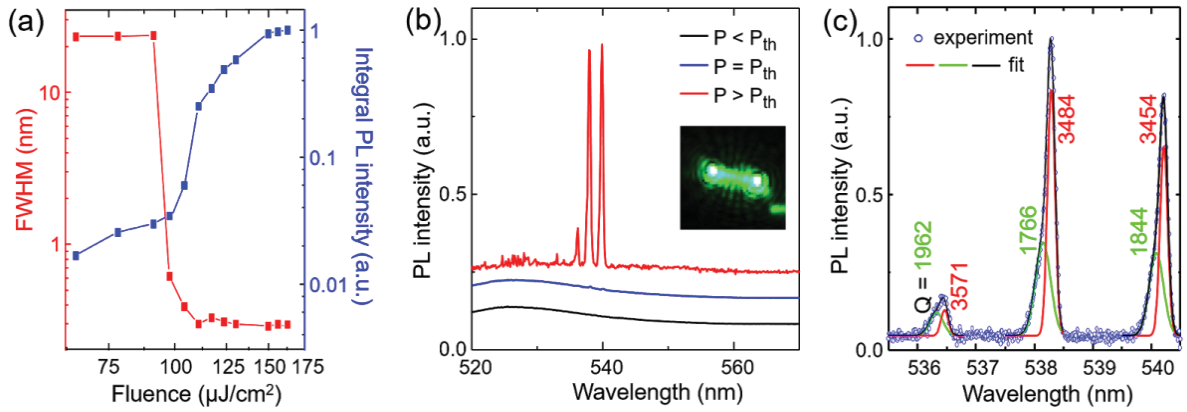

Figure 3. (a) Integral PL intensity and FWHM value versus excitation fluence relationship for 11.5 μm NW. (b) PL spectrum of the NW at different operation regimes (microphotograph of the acting nanolaser is presented in the inset image). (c) Gaussian fitting of the laser lines and Q-factors of the single modes.

Optical characteristics of mixed-halide perovskite samples were investigated in a similar way. It was found that under continuous weakly intense UV excitation films generate red light (λ_{em} = 630 nm) corresponding to the band gap energy $E_g \approx 2$ eV. Previously, Beal et al. reported a close value of E_g for $CsPbBr_{1.5}I_{1.5}$ perovskite.[17] In our experiments, PL QY of the iodine doped films at charge carrier density of $\approx 4.3 \cdot 10^{15}$ cm^{-3} equals to 9% approximately. In contrast to films demonstrating identical PL signals from different points over the entire surface, the luminescence of various mixed-halide NWs differed significantly because of the different cross-section of the structures. Since the efficient anion exchange between the perovskite crystal lattice and HI vapor mainly occurs at the crystal surface, NWs possessing a large cross-section undergo nonequivalent chemical transformation in their volume. On the contrary, crystals with a small cross-section are capable of uniform rehalogenation of the bulk. Further gradual annealing of the samples in the 150-320 °C temperature range leads to the mixing of various halogens in the bulk due to ion diffusion and formation of a certain phase of the mixed-halide perovskite. In addition, the annealing eliminates the major part of structural defects. This allows $CsPbBr_{3-x}I_x$ NWs to generate relatively intense spontaneous emission but no stimulated emission since the remaining part of the defects introduces strong nonradiative dissipation channels for photogenerated charge carriers. It should also be mentioned that measuring the PL QY from an array of $CsPbBr_{3-x}I_x$ NWs of certain chemical composition is not possible for the samples exposed to HI vapor. Therefore, taking into account the difference in PL QY between the tribromide and mixed-halide films, $CsPbBr_{1.5}I_{1.5}$ NWs which are considered below is roughly assumed to possess 3.7 times lower value ($\approx$22.5% at 6×10^{16} cm^{-3} charge carrier concentration) than that of $CsPbBr_3$ NWs.

When the mixed-halide samples were illuminated with intensive (P = 0.1 mW/μm^2) continuous wave (CW) light with photon energy above the band gap, they exhibited photoinduced phase instability resulting in the tuning of their PL spectrum over time. It was interesting to study the temperature dependence of the PL from mono- and mixed-halide

samples. For this purpose, a closed cycle cryostat and supercontinuum laser source with 488 and 532 nm bandpass filters for the excitation of $CsPbBr_3$ and $CsPbBr_{1.5}I_{1.5}$, respectively, were exploited. Cooling down the monohalide samples causes the following spectral changes: PL signal becomes narrower and more intensive while the position of the emission peak practically does not change (Fig. 4a, c). In the case of the $CsPbBr_{1.5}I_{1.5}$ film, it was found that the segregation effect manifesting itself in the appearance of two new emission bands in the spectrum at 620 and 680 nm is completely suppressed at 200 K (Fig. 4b). The short-wavelength light comes from perovskite domains enriched with Br^- ions, whereas long-wavelength emission is generated by domains with a high content of I^- ions.[19] In contrast to the mixed-halide film, NWs of similar chemical composition demonstrated no segregation effect at the temperature of 250 K (Fig. 4d). It is worth noting that when the excitation is removed the dark recovery of the light-induced phase separation proceeds in the same timescale as segregation evolves, which is 3-5 s for the mixed-halide films and NWs at 300 K, and about 7-8 min for the films cooled down to 250 K.

The observed difference between the temperatures at which mixed-halide phase of perovskite thin films and NWs becomes stable can be considered in terms of the crystal lattice defects diffusion. It is known that photoactivated halogen ions in halide perovskites migrate between lattice vacancies.[20] For this reason, the ion segregation rate is directly related to the diffusion rate of the vacancies determined in terms of diffusion coefficient $D = D_0\exp(-E_a/kT)$, where D_0 is a constant at $T \rightarrow \infty$, E_a is activation energy for vacancy diffusion, k is the Boltzmann constant. Furthermore, the concentration of vacancies also affects the segregation rate in an obvious way. From this point of view, initially monocrystalline perovskite NWs inherit a smaller number of defect states after the anion exchange procedure than polycrystalline thin films do. This explains enhanced resistance of the NWs against the ion segregation observed in the conducted experiments. Such a feature makes mixed-halide inorganic perovskite NWs attractive for the development of new photonic designs and optoelectronic devices emitting light over a wide spectral range.

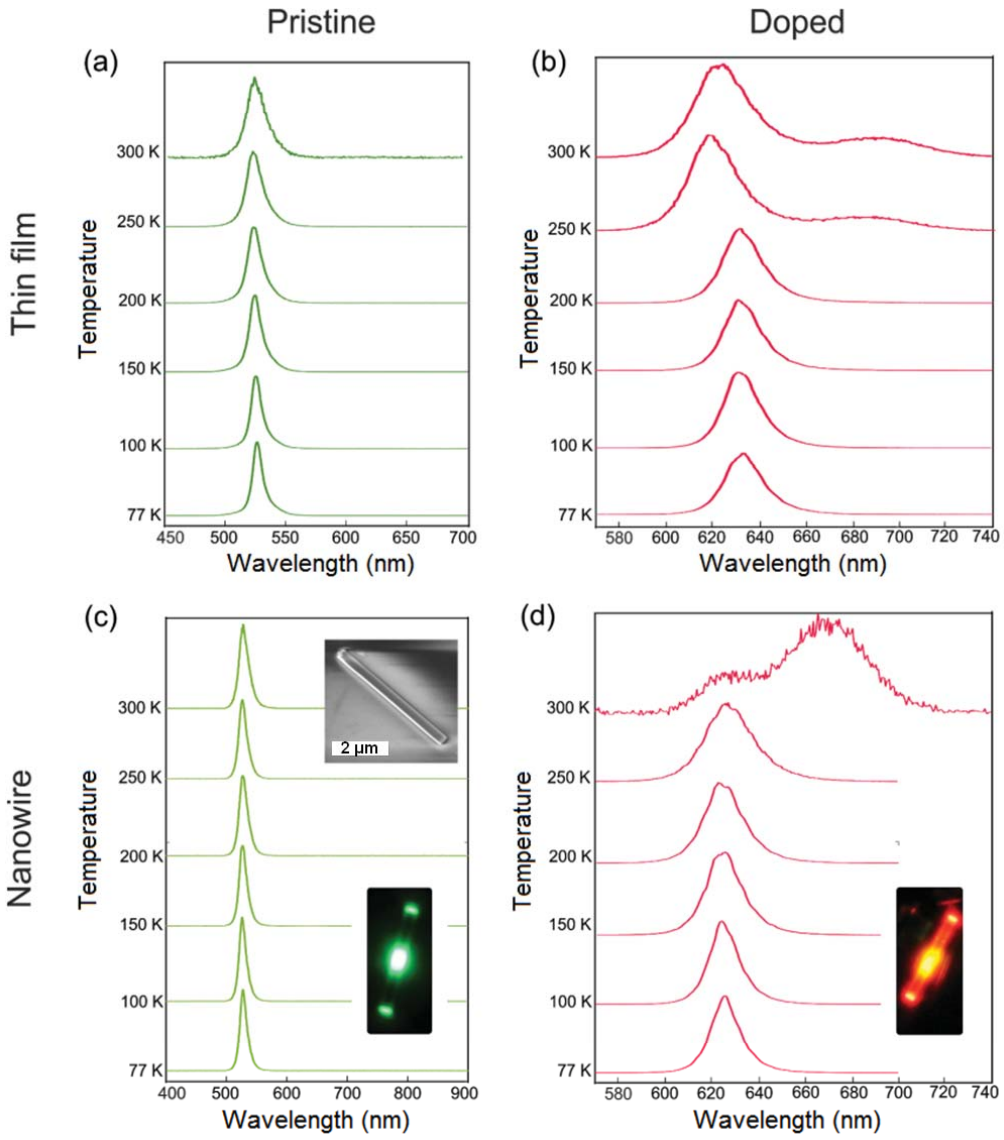

Figure 4. Dependence of the PL spectrum on temperature for $CsPbBr_3$ thin film (a) and NW (c) as well as for $CsPbBr_{1.5}I_{1.5}$ samples (b,d). Inset images: fluorescent microphotographs of the NW before (c) and after (d) the rehalogenation of its crystal structure; SEM image of the NW.

3. Conclusions

In summary, high-quality smooth thin films and monocrystalline nanowires of perovskite $CsPbBr_3$ have been fabricated by using improved wet chemical approaches. Additionally, the samples have been exposed to HI vapor to form related $CsPbBr_{1.5}I_{1.5}$ structures with narrower band gap. We have characterized all the obtained samples by means of scanning electron microscopy, stylus profilometry, X-ray photoelectron spectroscopy, X-ray powder diffraction, fluorescence and laser spectroscopy. The samples with mixed-halide composition have exhibited photoinduced phase instability upon continuous wave illumination, resulted in the dynamical modification of their optical characteristics, which can be suppressed under low temperature conditions. Since the phase instability is associated with the migration of photoactivated halogen ions (segregation) between perovskite lattice vacancies, the suppression of segregation at low temperatures occurs due to a decrease in the diffusion rate

of defect states. At the same time, perovskite NWs contain a lower concentration of structural vacancies than fine-grained films of the same chemical composition. For this reason, in comparison with thin films the stabilization of the phase and optical characteristics of mixed-halide perovskite nano- and microwires occurs at higher temperatures (about 250 K), that makes them promising materials for the development of new photonic designs and optoelectronic devices emitting light in the visible wavelength range.

3. Materials and methods

Materials. Lead(II) bromide ($PbBr_2$, 99.999%, Alfa Aesar), cesium bromide (CsBr, 99.999%, Sigma-Aldrich), dimethyl sulfoxide (DMSO, anhydrous, 99.8%, Alfa Aesar), isopropyl alcohol (IPA, technical grade, 95%, Vecton), hydrogen iodine (HI, 50%, Sigma-Aldrich) were used as received.

Preparation of perovskite ink. $PbBr_2$ (0.110 g, 0.3 mmol) and CsBr (0.07 g, 0.33 mmol) were dissolved in DMSO (3 ml) by shaking for 10 min to get a clear solution. Then the solution was filtered by using a 0.45 μm syringe filter with PTFE membrane. The chemicals were stored and mixed inside an N_2-filled glove box with both O_2 and H_2O level not exceeding 1 ppm.

$CsPbBr_3$ and $CsPbBr_{1.5}I_{1.5}$ thin films fabrication. Glass and hydrophobic silicon substrates were purchased from commercial suppliers. To make the substrates superhydrophilic, they were immersed in a piranha solution (mixture of 6 ml of sulfuric acid (H_2SO_4) and 2 ml of hydrogen peroxide (H_2O_2)) at 110 °C for 20 min. Afterwards substrates were carefully removed from the solution, rinsed with deionized water, dried with an air gun and then treated with ozone for 5 min.

To obtain high-quality films 30 μl of the perovskite ink was poured on the substrates and spin-coated at 2500 rpm for 300 s. To remove the residual DMSO molecules from the film, promote the complete conversion of the precursors to the target material $CsPbBr_3$, and eliminate the crystal lattice defects the deposited films were annealed gradually from 50 °C to 150 °C on a hot plate for 10 min.

In order to get thin films of mixed-halide composition, tribromide films were taken out of the glove box, then put in a Petri dish bottom and preheated with a glass piece lying close to the sample at 150 °C for 3 min. Afterwards, small amount of HI was dripped onto the glass piece and the sample with the glass were covered with the hot bottom of the weighing bottle. Thus the $CsPbBr_3$ film was exposed to hydrogen iodide vapor (5 μg/cm^3) at the temperature of 150 ˚C for 10 s. Finally, samples were gradually annealed in the 120–200 ˚C temperature range for 2 min to eliminate structural defects.

$CsPbBr_3$ and $CsPbBr_{1.5}I_{1.5}$ nanowires fabrication. The dissolved perovskite solution (0.1 M) was taken out from the glove box. The glass substrate was fixed in a plastic Petri dish bottom (35x9 mm) placed in a bigger glass one (80x15 mm) and preheated on the hotplate up to 50 °C. 0.5 μl of the ink was dripped onto a glass substrate with the formation of a small droplet. Immediately after that 100 μm of IPA•H_2O azeotrope was poured in the glass bottom and all the system was sealed. When the ink droplet increased in size due to the condensation of IPA•H_2O azeotrope on its surface, the substrate was tilted in such a way that the perovskite

droplet spreaded over the substrate leaving a trace. The trace was dried in the presence of IPA•H_2O azeotropic vapor for 1-2 min to give isolated high-quality NWs . This approach reduces the perovskite ink consumption and synthesis duration as compared to previously developed spray-casting at ambient conditions.[6]

To obtain NWs of the $CsPbBr_{1.5}I_{1.5}$ composition, the chemical vapor anion exchange method was used. The glass substrates with precipitated NWs were treated with HI vapor (5 μg/cm^3) at 150 °C for 30 s using the same construction as for chemical modification of the perovskite films. Afterwards, the samples were heated on a hotplate with a gradual increase in temperature from 150 to 320 °C for 2 minutes.

Structural characterization. Morphology of thin films and NWs were studied using a scanning electron microscope (Crossbeam 1540 XB, Carl Zeiss). High-resolution SEM images were obtained on FE-SEM-FIB HELIOS Nanolab 650 (FEI). Roughness of thin films was measured on a stylus profiler (P-7, KLA-Tencor). XRD patterns were measured using an X-ray diffractometer (SmartLab, Rigaku) equipped with a 9 kW rotating Cu anode X-ray tube. The measurements were performed using the grazing incidence (GIXRD) method in the 2θ range of 10-50^o. The angle between the X-ray primary beam and the specimen surface was adjusted to 0.5^o. XPS spectra were measured at $2.4x10^{-9}$ mbar pressure on X-ray photoelectron spectrometer system (Thermo Scientific K-Alpha) equipped with an Al source of monochromatic K-alpha X-ray (*hv* = 1486.6 eV). An energy scale was adjusted in accordance with Au 4f = 84 eV, Ag 3d = 368.2 eV and Cu 2p = 932.6 eV lines of standard samples. To neutralize a surface charge, a calibrated (C 1s = 284.8 eV) compensating electron flood gun was used. To obtain high-resolution (0.1 eV resolution) spectra, the x-ray beam was focused to 200 μm spot at constant pass energy of 50 eV and the number of scans of 10 was chosen.

Optical characterization. Spontaneous emission spectra of perovskite thin films and single NWs were recorded by using optical fiber spectrometer (Ocean Optics QE Pro) coupled with a microscope (Axio Imager A2m, Carl Zeiss) operating in the fluorescent regime. PL QY of perovskite thin films was measured in an integrating sphere under 368 nm CW excitation corresponding to photoexcited carrier density of $\approx 4.3 \cdot 10^{15}$ cm^{-3}. PL QY of $CsPbBr_3$ was derived from PL decay (Fig. S3) measured using the Edinburgh Instruments time-correlated single photon counting fluorescence spectrometer F900. The picosecond pulsed diode laser EPL-375 emitting 50 ps pulses at 375 nm with a repetition rate of 20 MHz was used for the sample excitation. The time resolution of the setup was found to be about hundred of picoseconds by applying apparatus function deconvolution.

Lasing from single NWs was investigated on a home-built optical setup (Fig. S4). Amplified femtosecond Yb:KGW laser (Pharos, Light Conversion) was used as an excitation source. Its output of 220 fs pulses arriving at 25 kHz repetition rate was frequency tripled in a home-built third harmonic generator and the resulting 343 nm beam was used to excite the sample. The excitation beam was focused onto the sample surface at normal incidence by the UV fused silica lens L1 (f=100 mm) which ensured a near-Gaussian excitation spot with a FWHM of 50 μm. The excitation pulse energy could be attenuated between 120 nJ and 1.2 nJ using a variable neutral density filter. The power was measured before the focusing lens L1 by a power meter (Ophir Nova2) equipped with a thermal power sensor (Ophir 3A). Emission of a single NW was collected in transmission configuration using 50× microscope objective (Mitutoyo M-Plan APO NUV, NA = 0.42) and passed through a long-pass filter with a cut-on

wavelength of 450 nm to block the excitation light. The emission was then directed into a high resolution spectrograph (Andor Shamrock SR-500i) equipped with a sensitive CCD camera (Andor iXON-DU-885). A grating of 1650 grooves/mm and input slit setting of 10-20 μm ensured the spectral resolution of around 45 pm. Sample positioning in the excitation beam was aided by a widefield microscope operated in epi-illumination arrangement, in which white LED served as an excitation source and a small color CCD camera (Point Grey Chameleon) was used to monitor the image through a beam splitter BS. Flipper mirror FM1 allowed switching between sample positioning and spectrum recording modes. All measurements were performed at ambient conditions.

Acknowledgment

The authors thank Dr. Vidas Pakštas, Arnas Naujokaitis, Filipp Komissarenko and Soslan Khubezhov for the help in the samples characterization. S.V.M. and A.A.Z. thank the Russian Science Foundation (grant 17-73-20336) for the financial support of study of nanostructures. S.V.M. acknowledges funding from the Ministry of Science and Higher Education of the Russian Federation (project 14.Y26.31.0010). M.V. acknowledges funding from the European Regional Development Fund according to the supported activity 'Research Projects Implemented by World-class Researcher Groups' under Measure No. 01.2.2-LMT-K-718, grant No. 01.2.2-LMT-K-718-01-0014. G.H. acknowledges ITMO Fellowship Program.

References:

[1] L. Protesescu, S. Yakunin, M.I. Bodnarchuk, F. Krieg, R. Caputo, C.H. Hendon, R.X. Yang, A. Walsh, and M.V. Kovalenko, Nano Lett. **15**, 3692 (2015).
[2] L.M. Herz, ACS Energy Lett. **2**, 1539 (2017).
[3] NREL. Efficiency chart. https://www.nrel.gov/pv/cell-efficiency.html
[4] W. Xu, Q. Hu, S. Bai, C. Bao, Y. Miao, Z. Yuan, T. Borzda, A.J. Barker, E. Tyukalova, Z. Hu, M. Kawecki, H. Wang, Z. Yan, X. Liu, X. Shi, K. Uvdal, M. Fahlman, W. Zhang, M. Duchamp, J.-M. Liu, A. Petrozza, J. Wang, L.-M. Liu, W. Huang, and F. Gao, Nature Photonics, (2019), DOI: 10.1038/s41566-019-0390-x.
[5] S. Makarov, A. Furasova, E. Tiguntseva, A. Hemmetter, A. Berestennikov, A. Pushkarev, A. Zakhidov, and Y. Kivshar, Adv. Opt. Mater. **7**, 1800784 (2019).
[6] A.P. Pushkarev, V.I. Korolev, D.I. Markina, F.E. Komissarenko, A. Naujokaitis, A. Drabavičius, V. Pakštas, M. Franckevičius, S.A. Khubezhov, D.A. Sannikov, A.V. Zasedatelev, P.G. Lagoudakis, A.A. Zakhidov, and S.V. Makarov, ACS Appl. Mater. Interfaces **11**, 1040 (2019).
[7] H. Zhu, Y. Fu, F. Meng, X. Wu, Z. Gong, Q. Ding, M.V. Gustafsson, M.T. Trinh, S. Jin, and X.-Y. Zhu, Nature Mater. **14**, 636 (2015).
[8] Y. Fu, H. Zhu, A.W. Schrader, D. Liang, Q. Ding, P. Joshi, L. Hwang, X.-Y. Zhu, and S. Jin, Nano Lett. **16**, 1000 (2016).
[9] S.W. Eaton, M. Lai, N.A. Gibson, A.B. Wong, L. Dou, J. Ma, L.-W. Wang, S.R. Leone, and P. Yang, PNAS **113**, 1993 (2016).
[10] L. Jiang, R. Liu, R. Su, Y. Yu, H. Xu, Y. Wei, Z.-K. Zhou, and X. Wang, Nanoscale **10**, 13565 (2018).
[11] K. Park, J.W. Lee, J.D. Kim, N.S. Han, D.M. Jang, S. Jeong, J. Park, and J.K. Song, J. Phys. Chem. Lett. **7**, 3703 (2016).
[12] E.T. Hoke, D.J. Slotcavage, E.R. Dohner, A.R. Bowring, H.I. Karunadasa, and M.D. McGehee, Chem. Sci. **6**, 613 (2015).

[13] N.J. Jeon, J.H. Noh, Y.C. Kim, W.S. Yang, S. Ryu, and S.I. Seok, Nature Materials **13**, 897 (2014).
[14] J. Li, X. Shan, S.G.R. Bade, T. Geske, Q. Jiang, X. Yang, and Z. Yu, J. Phys. Chem. Lett. **7**, 4059 (2016).tiguntseva
[15] M. Rodová, J. Brožek, K. Knížek, and K. Nitsch, J. Therm. Anal. Calorim. **71**, 667 (2003).
[16] E.Y. Tiguntseva, D.G. Baranov, A.P. Pushkarev, B. Munkhbat, F. Komissarenko, M. Franckevičius, A.A. Zakhidov, T. Shegai , Y.S. Kivshar, and S.V. Makarov, Nano Lett. **18**, 5522 (2018).
[17] R.E. Beal, D.J. Slotcavage, T. Leijtens, A.R. Bowring, R.A. Belisle, W.H. Nguyen, G.F. Burkhard, E.T. Hoke, and M.D. McGehee, J. Phys. Chem. Lett. **7**, 746 (2016).
[18] T.G. Liashenko, E.D. Cherotchenko, A.P. Pushkarev, V. Pakstas, A. Naujokaitis, S.A. Khubezhov, R.G. Polozkov, K.B. Agapev, A.A. Zakhidov, I.A. Shelykh, S.V. Makarov, Phys. Chem. Chem. Phys., 21, 18930 (2019)
[19] S.J. Yoon, S. Draguta, J.S. Manser, O. Sharia, W.F. Schneider, M. Kuno, and P.V. Kamat, ACS Energy Lett. **1**, 290 (2016).
[20] A. Ruth, M.C. Brennan, S. Draguta, Y.V. Morozov, M. Zhukovskyi, B. Janko, P. Zapol, and M. Kuno, ACS Energy Lett. **3**, 2321 (2018).

Supporting information

Photophysical properties of halide perovskite $CsPb(Br_{1-x}I_x)_3$ thin films and nanowires

D.I. Markina,[1]* E.Yu. Tiguntseva,[1] A.P. Pushkarev,[1] M.A. Samsonov,[2] M. Vengris,[3] B. Munkhbat,[4] T. Shegai,[4] G. Hix,[5] A.A. Zakhidov,[1,6] S.V. Makarov[1]

[1] ITMO University, 197101 St.Petersburg, Russia
[2] University of Pardubice, 532 10 Pardubice, Czech Republic
[3] Vilnius University, LT-10223 Vilnius, Lithuania
[4] Chalmers University of Technology, SE-412 96 Gothenburg, Sweden

[5] *University of Wolverhampton, WV1 1LY Wolverhampton, United Kingdom*
[6] *The University of Texas at Dallas, Richardson, 75080 TX, USA*

Corresponding author: D.I. Markina daria.markina@metalab.ifmo.ru , A.P. Pushkarev anatoly.pushkarev@metalab.ifmo.ru

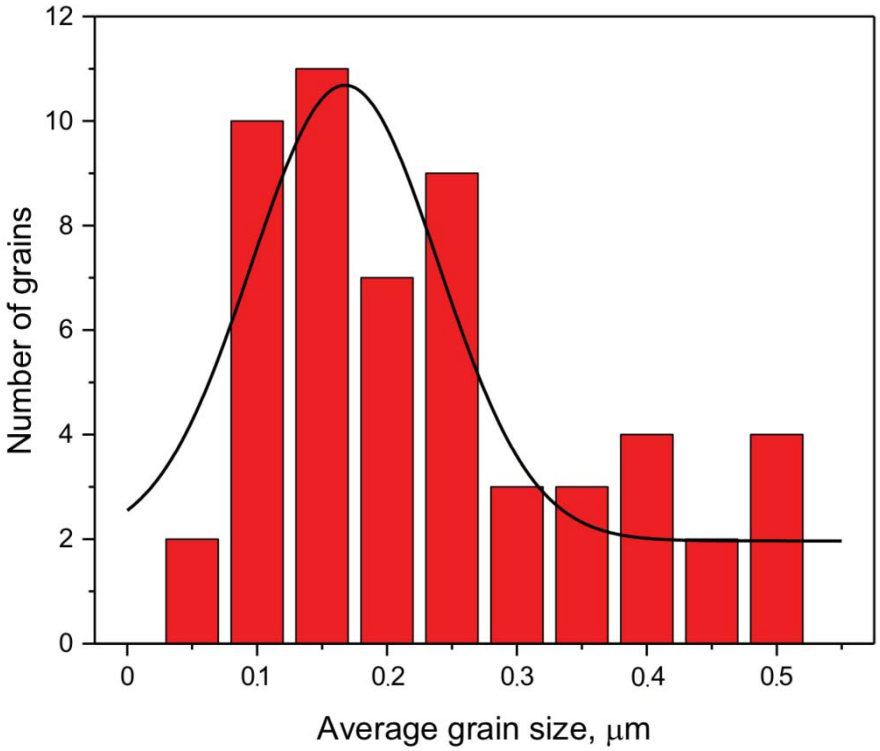

Figure S1. Average grain size distribution.

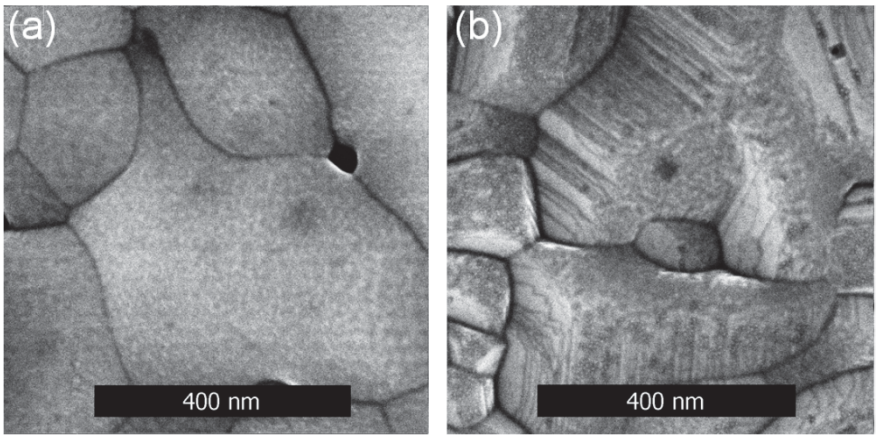

Figure S2. High-resolution SEM images of $CsPbBr_3$ (a) and $CsPbBr_{1.5}I_{1.5}$ (b) thin films.

S3. PL QY estimation for $CsPbBr_3$ NWs

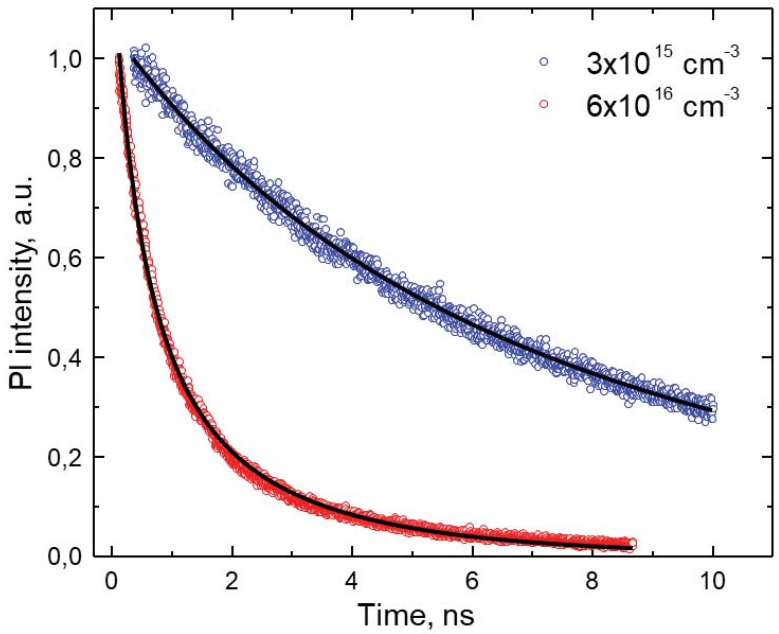

Figure S3. Photoluminescence decay of $CsPbBr_3$ NWs at different densities of the generated charge carriers.

PL QY of $CsPbBr_3$ NWs was estimated by using AB model discussed in detail in previous report.[7] The estimation is based on the fitting PL decay (Fig. S3) by fluence dependent bimolecular recombination function (1) from which, at given density of initially generated electron-hole pairs (n_0), a carrier trapping rate constant (A) and electron-hole radiative recombination rate constant (B) can be determined:

$$n(t) = \frac{n_0 \exp(-At)}{1 + n_0 \frac{B}{A}(1 - \exp(-At))}. \quad (1)$$

These constants are used to obtain PL QY (2) at n_0 lower than charge carriers concentration causing Auger recombination:

$$QY_{PL} = \frac{Bn_0}{A + Bn_0}. \quad (2)$$

n_0 is derived from the given excitation fluence, average thickness of the NWs which is about 0.5 μm, and attenuation coefficient $\alpha = \frac{4\pi}{\lambda} \mathrm{Im}(n(\omega))$ obtained from dispersion curves for $CsPbBr_3$.[16] It was found out, that carrier density ≈ 3×10^{15} cm^{-3} gives A = 9.2×10^{7} s^{-1}, B = 2.2×10^{-8} s^{-1} cm^3, and QY ≈ 41.7%, whereas n_0 ≈ 6×10^{16} cm^{-3} provides A = 2.94×10^{8} s^{-1}, B = 2.47×10^{-8} s^{-1} cm^3, and QY ≈ 83.4%.

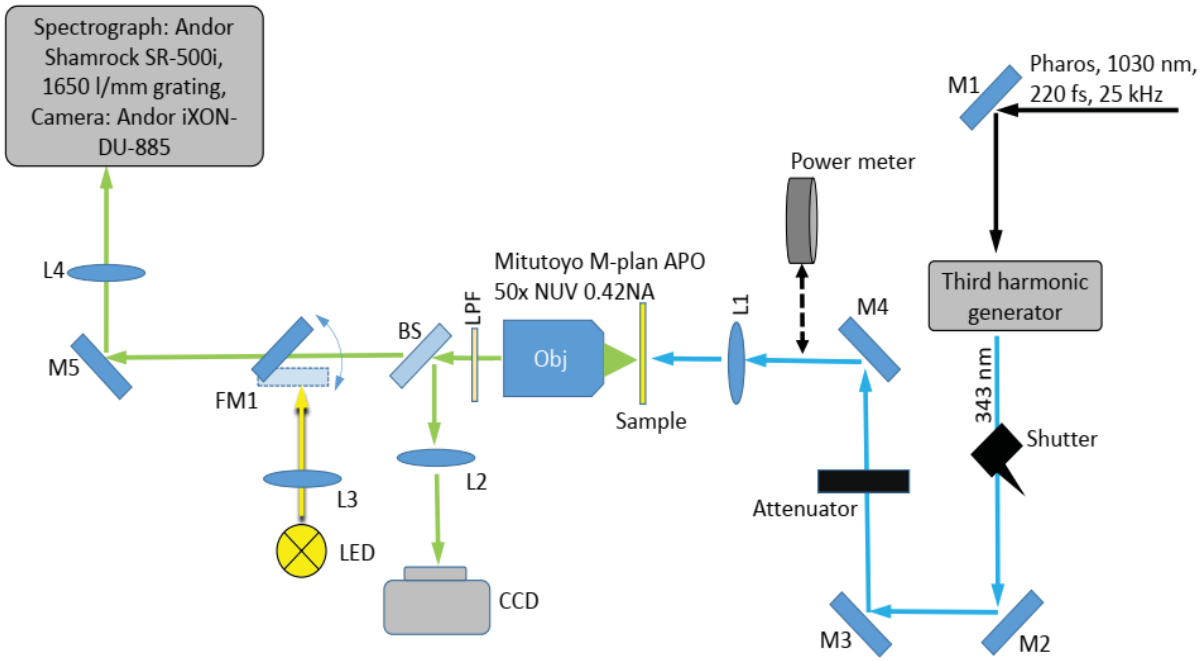

Figure S4. Schematic representation of the home-built optical setup employed for the detection of lasing from the perovskite nanowires. M1-M5: mirrors, Attenuator – variable neutral density filter, L1-L3 lenses, BS – beamsplitter, FM1 – flipper mirror.

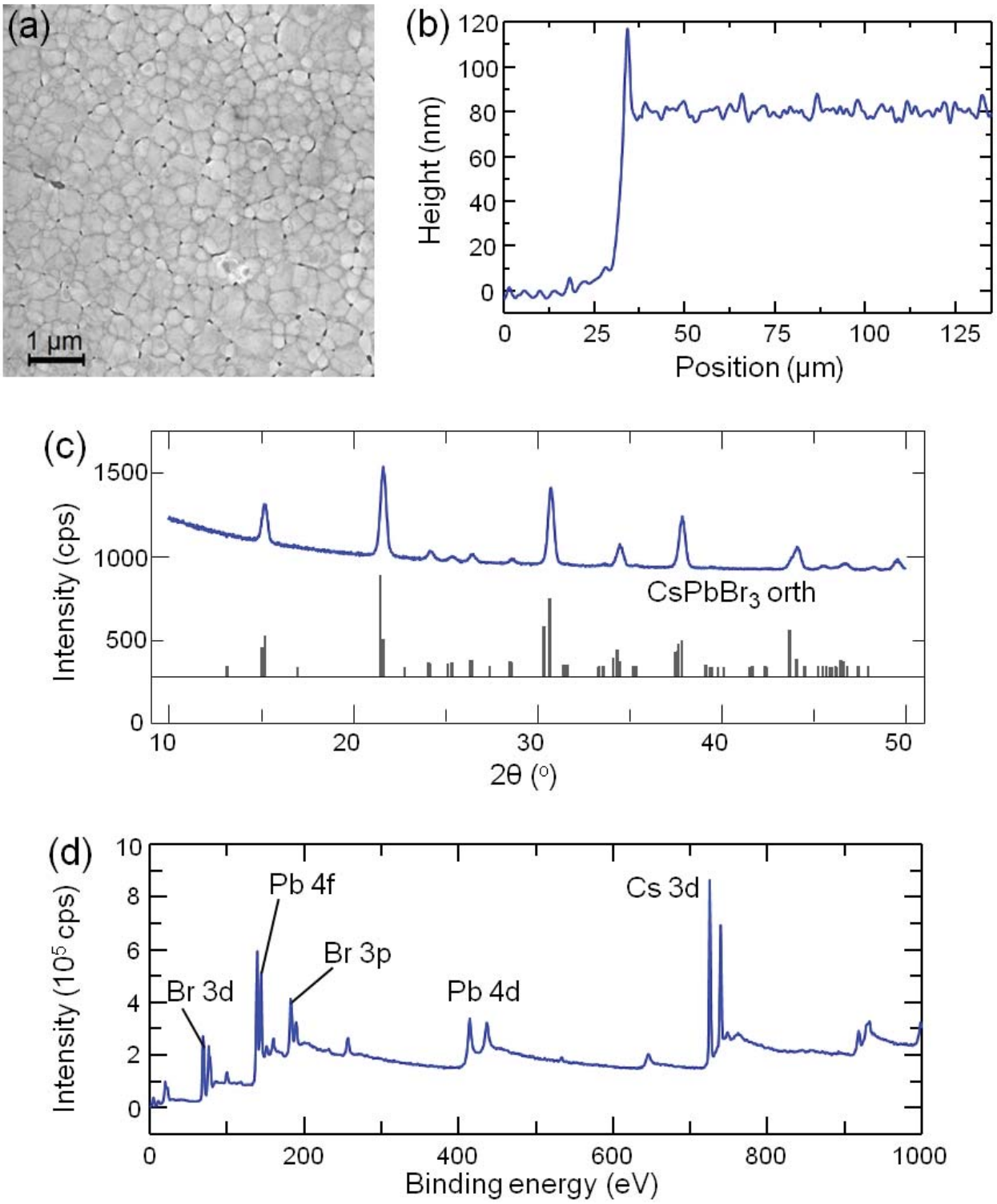
(a)
1 μm
(b)
Height (nm)
Position (μm)
(c)
Intensity (cps)
CsPbBr3 orth
2θ (°)
(d)
Intensity (10^5 cps)
Pb 4f
Br 3p
Br 3d
Pb 4d
Cs 3d
Binding energy (eV)

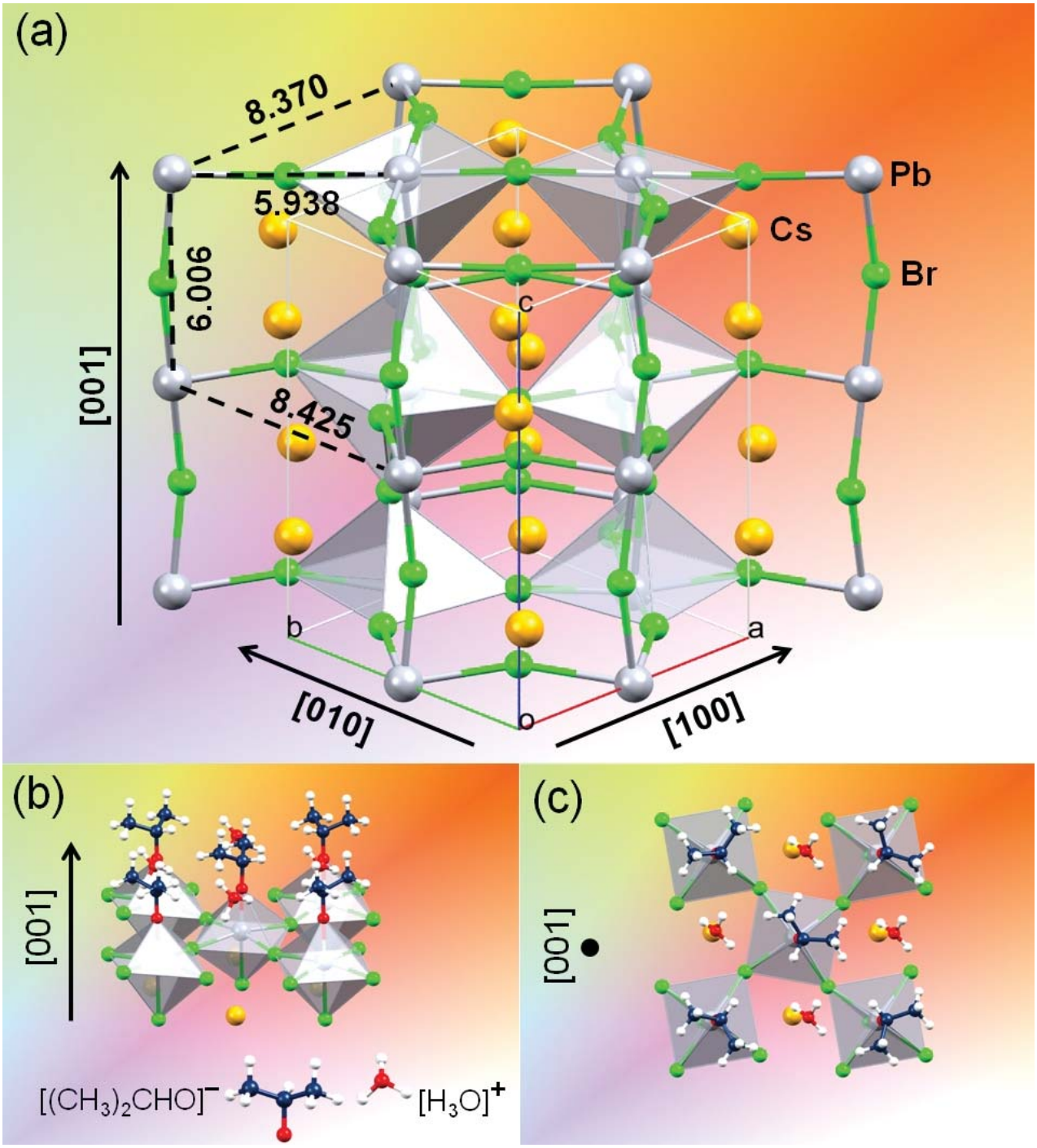
(a)
8.370
5.938
6.006
8.425
[001]
Pb
Cs
Br
c
b
a
[010]
[100]
(b)
[001]
[(CH3)2CHO]−
[H3O]+
(c)
[001]

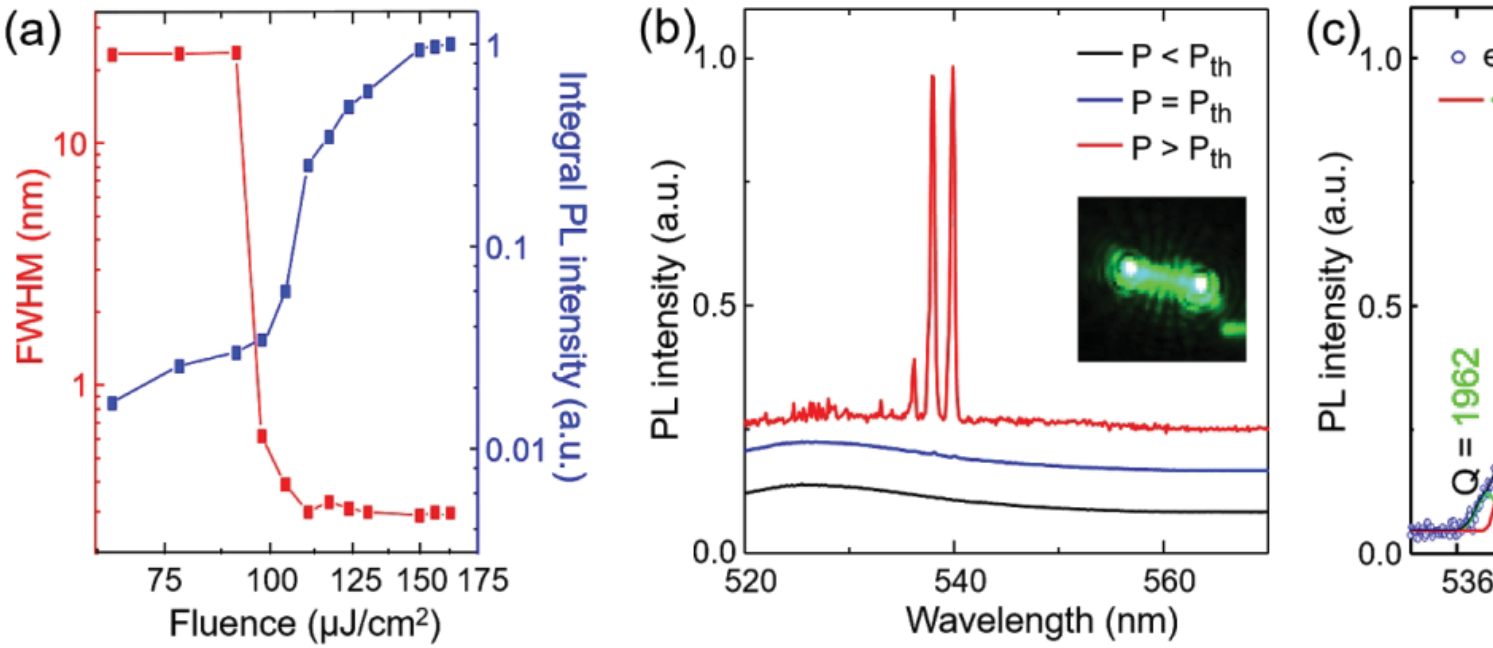
(a)
FWHM (nm)
10
1
Integral PL intensity (a.u.)
1
0.1
0.01
75
100
125
150
175
Fluence (μJ/cm²)
(b)
1.0
0.5
0.0
PL intensity (a.u.)
P < Pth
P = Pth
P > Pth
520
540
560
Wavelength (nm)
(c)
1.0
0.5
0.0
PL intensity (a.u.)
Q = 1962
536

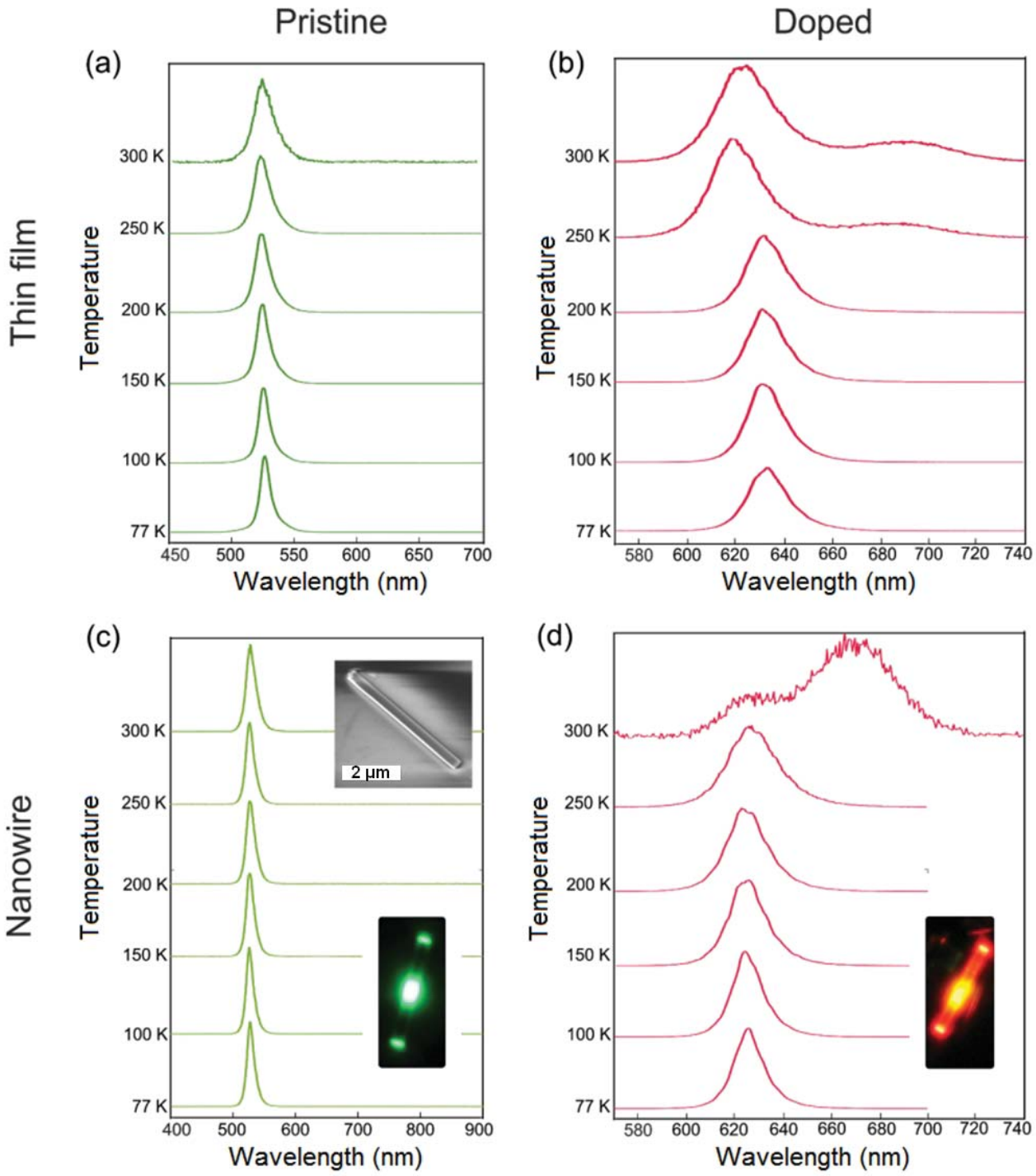
Pristine
Doped
Thin film
Nanowire
(a)
(b)
(c)
(d)
300 K
250 K
200 K
150 K
100 K
77 K
Temperature
Wavelength (nm)
2 μm

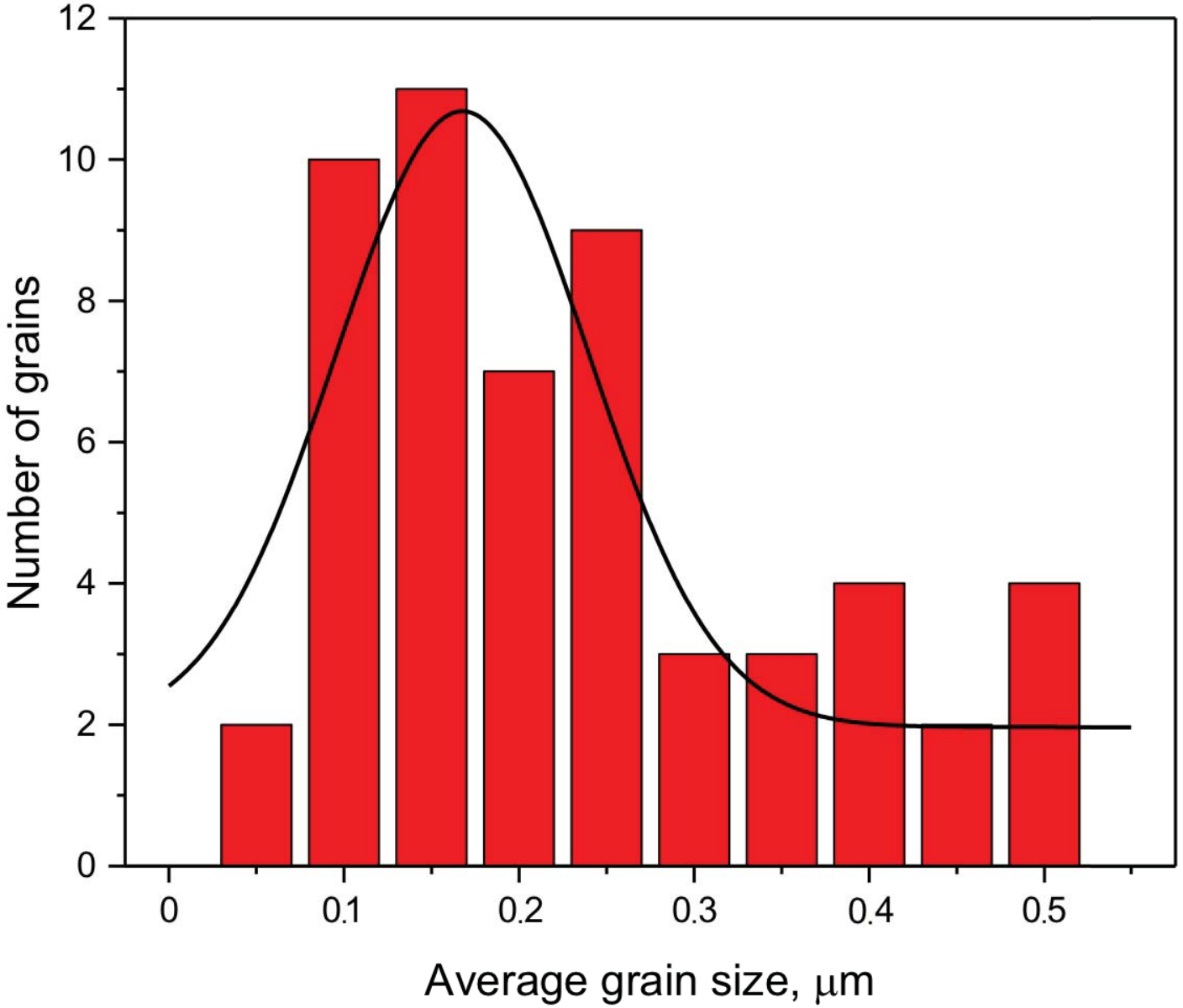
Number of grains
Average grain size, μm
0
2
4
6
8
10
12
0
0.1
0.2
0.3
0.4
0.5

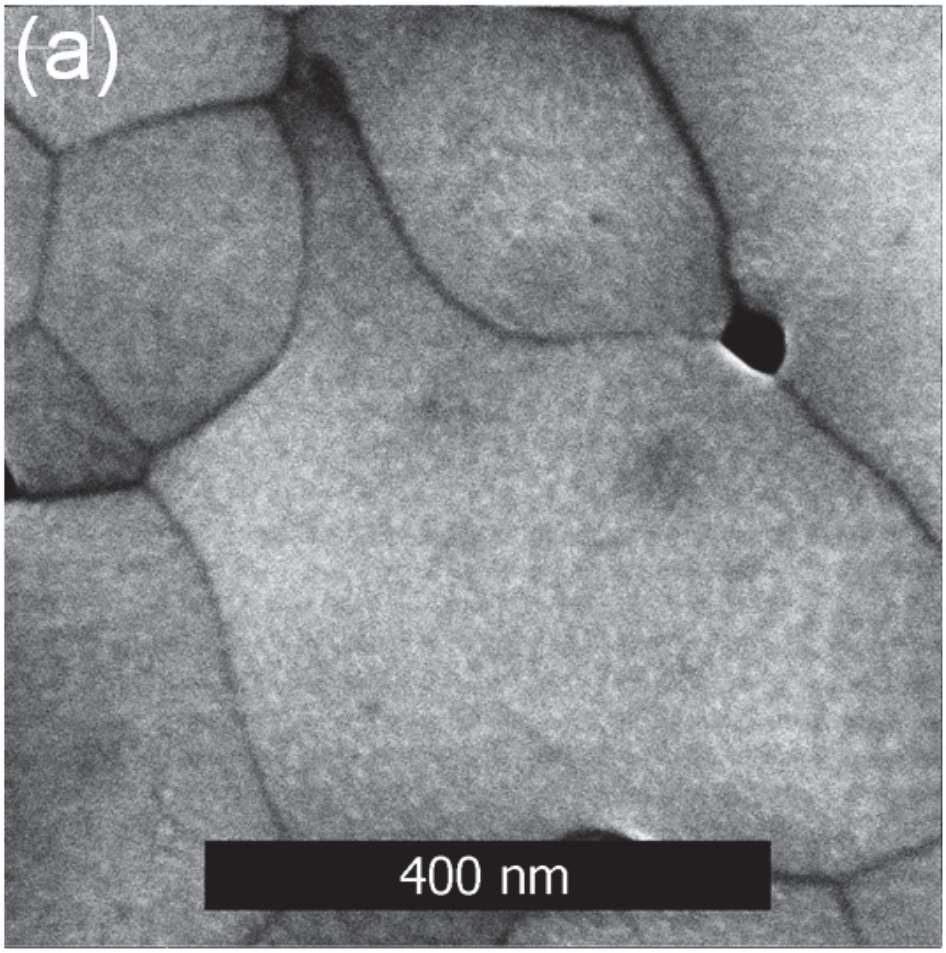
(a)
400 nm

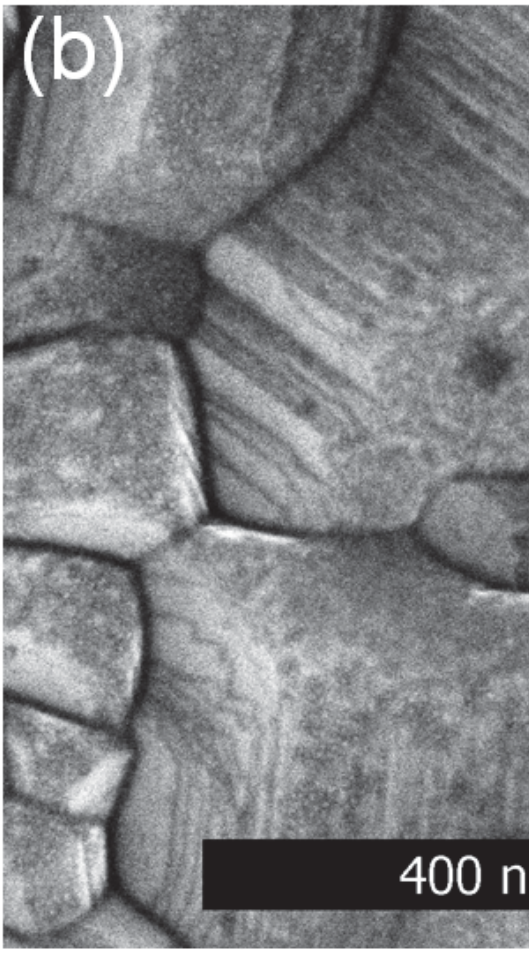
(b)
400 n

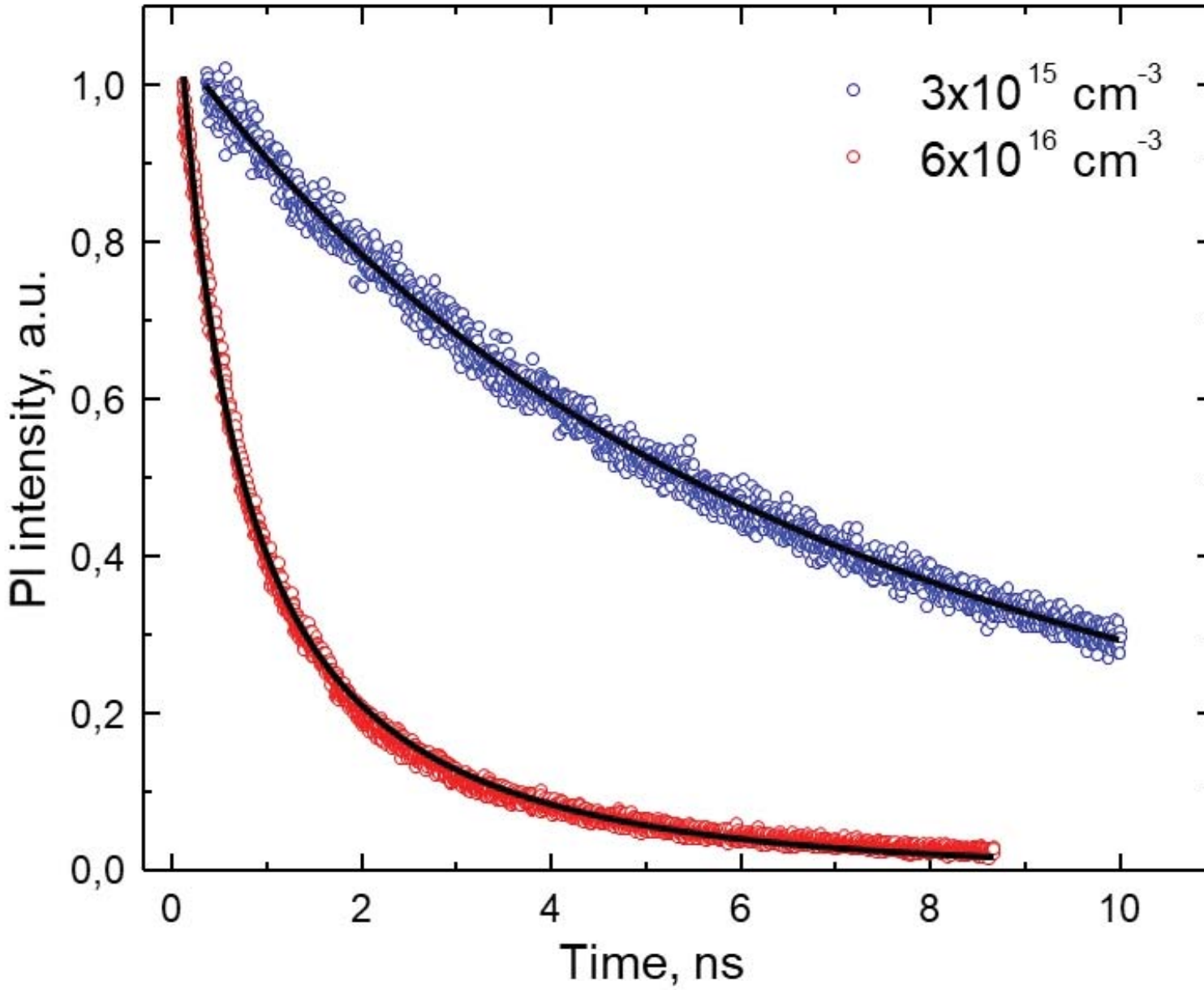
3x10^15 cm^-3
6x10^16 cm^-3
PI intensity, a.u.
Time, ns
0,0
0,2
0,4
0,6
0,8
1,0
0
2
4
6
8
10

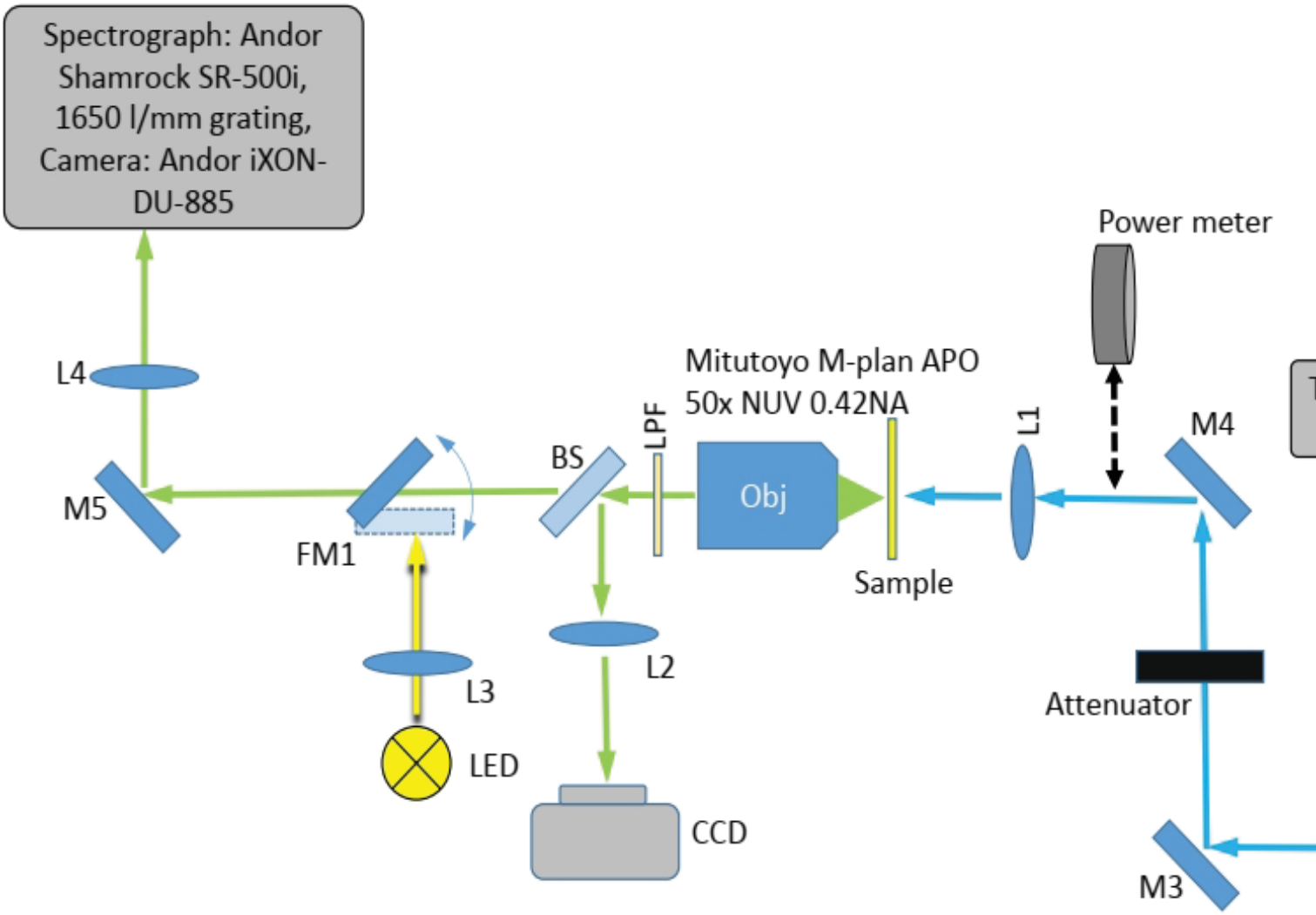
Spectrograph: Andor Shamrock SR-500i, 1650 l/mm grating, Camera: Andor iXON-DU-885
L4
M5
FM1
BS
LPF
Mitutoyo M-plan APO 50x NUV 0.42NA
Obj
Sample
L1
Power meter
M4
L3
LED
L2
CCD
Attenuator
M3

The authors declare no conflict of interests.